INTEGRATED PROJECTIONS OF RELATIVE SEA-LEVEL RISE AND LAND SUBSIDENCE IN THE GULF OF THAILAND: A BIAS-CORRECTED APPROACH

INTEGRATING HISTORICAL DATA AND FUTURE SCENARIOS FOR COASTAL VULNERABILITY ASSESSMENTS

INTEGRATED PROJECTIONS OF RELATIVE SEA-LEVEL RISE AND LAND SUBSIDENCE IN THE GULF OF THAILAND: A BIAS-CORRECTED APPROACH

INTEGRATING HISTORICAL DATA AND FUTURE SCENARIOS FOR COASTAL VULNERABILITY ASSESSMENTS
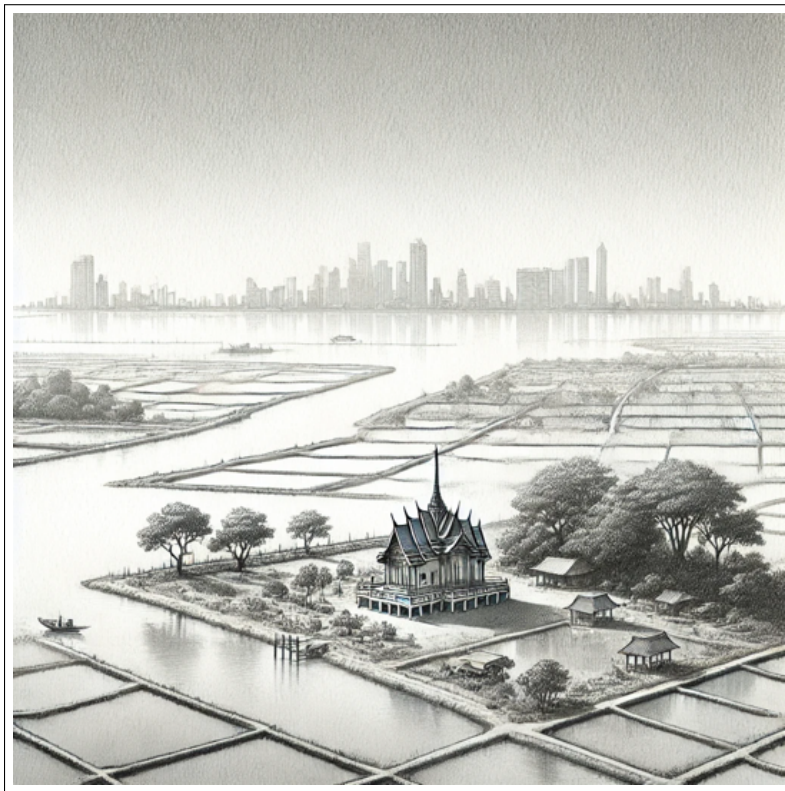
Scriptie

ter verkrijging van de graad van Msc aan de Technische Universiteit Delft,
te verdedigen op donderdag 8 augustus 2024 om 10:30 uur

door

Tijmen Samuel DE BOER

Deze scriptie is goedgekeurd door de

Prof. dr. ir. F.C. Vossepoel
Ir. W.J.F. Simons

Samenstelling beoordelingscommissie:

Prof. dr. ir. F.C. Vossepoel,   Technische Universiteit Delft
ir. W.J.F. Simons,   Technische Universiteit Delft

Onafhankelijke leden:
Dr. ir. A.B.A. Slangen   NIOZ

CONTENTS

LIST OF FIGURES

LIST OF TABLES

EXECUTIVE SUMMARY

In this thesis, I investigate the impact of sea-level rise (SLR) and land subsidence on coastal vulnerability in the Gulf of Thailand. I have focused on the region south of Bangkok around the Chao Phraya River in Samut Prakan province. This area is of interest due to its economic importance, dense population, and ecological diversity. The region faces increasing threats from climate change. In this study, I aim to integrate historical sea-level data from Global Climate Models (GCMs) and tide gauge stations with future scenarios to assess coastal vulnerability. I use a bias-corrected approach to refine projections of sea-level rise.

The study begins with a detailed historical analysis of sea levels in the Gulf of Thailand, using tide gauge data from four stations in the Gulf of Thailand. This data, spanning several decades, provides a baseline for understanding long-term trends in sea-level changes and seasonal variations and irregularities necessary for global model adjustments. Three bias correction methods-linear scaling, variance scaling and quantile mapping— have been used to adjust outputs from 12 CMIP5 historical climate models, ensuring their predictions align with local conditions.

Using the most effective bias correction method, linear scaling, future sea-level changes under Representative Concentration Pathways SSP4.5 and SSP8.5 have been adjusted. These scenarios have been extracted from the IPCC AR6 report (Lee and Romero, 2023). SSP4.5 represents a stabilisation scenario with emissions peaking around 2040 and then declining, while SSP8.5 assumes a high-emission scenario with continuous increases throughout the 21st century. These projections are refined to a monthly resolution, considering seasonal fluctuations observed in historical data, increasing the reliability of predictions for regional planning. These scenarios are expressed with confidence intervals, highlighting possible outcomes and their probabilities.

Thereafter, ground deformation scenarios are extrapolated for ten locations in the study area, based on historical land movement data from three sites. This allows for an elevation map to be combined with sea-level projections, providing a better understanding of future coastal impacts.

Based on this study, it can be concluded that the Gulf of Thailand experiences unique local phenomena that can differ from global trends, such as the influence of monsoon winds and local bathymetry on sea-level fluctuations. The presence of these local phenomena emphasises the importance of localising global sea level rise predictions by incorporating regional factors. For the Gulf of Thailand these factors include seasonal monsoon winds and detailed bathymetric data.

One significant finding is that despite substantial projected sea-level rise, the difference in flooding extent between lower and upper scenarios is less pronounced than expected. This suggests that local factors, such as topography and land subsidence, may play a more significant role in determining flooding extent. The research identifies limitations in the availability of tide gauge data, suggesting that integrating land subsidence data at these stations could enhance accuracy.

Overall, the outcome of this study underscores the necessity of incorporating local data and refining global models for regional applications. It contributes to understanding the compounded effects of SLR and land subsidence on coastal vulnerability in the Gulf of Thailand and provides insights into effective climate adaptation strategies for similar coastal regions globally.

1

INTRODUCTION

In recent years, coastal vulnerability in southern Bangkok has become a pressing issue due to the combined effects of sea-level rise and land subsidence. The region's economic significance, dense population, and unique ecological systems are increasingly threatened by changing climatic conditions. Addressing these concerns can only be accomplished with a comprehensive understanding of the impacts of sea-level rise and subsidence, particularly in coastal regions where the risks posed by climate change are escalating.

Global studies on sea-level rise and subsidence have mainly focused on overarching trends and projections. The Intergovernmental Panel on Climate Change (IPCC) reports that the global mean temperature has increased by approximately 1°C since pre-industrial levels and is expected to reach 1.5°C by 2030–2052 (Intergovernmental Panel on Climate Change, 2023). This temperature rise has led to the thermal expansion of seawater and the melting of glaciers and ice sheets, causing a significant rise in global mean sea levels since the early 1970s (Church and White, 2011). The rate of global mean sea-level rise (SLR) increased from 1.7 mm/year between 1901 and 1993 to 3.2 mm/year from 1993 to 2010, primarily due to ocean thermal expansion and changes in glaciers and ice sheets (Nerem et al., 2022). This upward trend is likely to continue with further increases in temperature (Slangen et al., 2014).

SLR has numerous damaging effects, such as storm surges, erosion, and saltwater intrusion into coastal regions. These impacts affect tidal currents in many estuaries, increase salinity in surface water and groundwater systems and threaten domestic and agricultural water supplies. These effects are predominately experienced in regions such as the Apalachicola River in the USA, the Gorai River in Bangladesh, the Puzih River in Taiwan, and the Chao Phraya River in Thailand. Excessive groundwater pumping in coastal areas increases land subsidence, further increasing the threat of flooding and seawater intrusion into groundwater systems. Studies have shown that the combined effects of SLR and land subsidence, mainly driven by excessive groundwater abstraction, may increase these issues in several coastal regions (Saramul and Ezer, 2014).

In Bangkok, the capital city of Thailand, the impacts of these phenomena are partic-

ularly pronounced. The city's population of over 11 million relies heavily on the Chao Phraya River for its freshwater supply. Over the past several decades, rapid industrial development in Bangkok and its surrounding provinces has significantly increased the demand for water, especially from industries. While groundwater in Bangkok is of good quality and quantity, excessive pumping — reaching up to 2.2 Mm^3/d in 1999 — has caused substantial land subsidence. In the early 1980s, subsidence rates exceeded 120 mm/year, though this rate decreased to 10 mm/year in the 2000s. Groundwater extraction-induced land subsidence has emerged as a serious issue not only in Bangkok, also other regions such as the Mekong Delta (Trisirisatayawong et al., 2011).

Studies investigating tidal data and altimetry measurements in the Gulf of Thailand (GoT) have found that relative sea level is rising significantly faster than global average rates, with land subsidence due to excessive groundwater extraction and earthquakes being major contributors (Trisirisatayawong et al., 2011). The contribution of earthquakes is demonstrated by the 2004 Mw 9.2 Sumatra-Andaman earthquake, which had a profound impact on the tectonic landscape of Thailand. This megathrust earthquake caused rapid upward motion of the Burma microplate, part of the larger Sunda Plate on which Thailand is located. The event resulted in temporary tectonic land subsidence in regions closer to the trench, such as Phuket. The region in the Northern part of the Gulf of Thailand experienced less pronounced effects of the earthquake. The earthquake initiated a cycle of crustal deformation that continues to influence relative sea levels along Thailand's coasts, contributing to long-term changes in the region's tectonic landscape (Naeije et al., 2022).

To mitigate these issues, it is important to understand future changes in SLR under changing climate conditions. Previous studies have projected SLR based on various climate change scenarios but often without considering biases in global climate model (GCM) data. These biases arise due to differences between various data sets, between different models, and discrepancies between observational data and model outputs. By combining historical data, satellite observations, and different climate models, I aim to reduce these biases and generate forecasts that are as realistic as possible. The goal is to provide a comprehensive understanding of future coastal changes to inform effective adaptation strategies.

In this study, I have adapted localised sea-level projections for the entire Gulf of Thailand, considering both regional and global influences. While the models will encompass the entire Gulf, specific coastal impact scenarios will focus on the province of Samut Prakan. This is the province located south of Bangkok.

1.1. RESEARCH QUESTION

The primary research question guiding this study is:

How will relative sea-level rise, considering both uncertainties in climate change and local land subsidence, affect the coastline in the province of Samut Prakan?

Addressing this question is vital for anticipating and mitigating the future impacts of climate change on coastal regions, which are increasingly susceptible to both natural and anthropogenic factors.

1.2. Sub-questions

To address the primary research question, the study is divided into the following sub-questions:

- What are the historical rates of relative sea-level rise observed in the Gulf of Thailand?

- How can CMIP5 historic model outputs be combined with observed tide gauge data to adjust for local circumstances?

- How does the sea-level range of these adjusted outputs inform us about the expected local sea-level changes given the SSP 4.5 and SSP 8.5 scenarios, and how can these projections be expressed in terms of confidence intervals?

- Based on the adjusted sea-level rise projections and land subsidence scenarios, what coastline scenarios can be expected for the Samut Prakan and what would be the probability for these scenarios?

1.3. Research Structure

The research methodology is designed to systematically address the research question and sub-questions. The structure of the research is as follows (Figure 1.1):

Historical Analysis: The study begins with a detailed analysis of historical sea levels in the Gulf of Thailand. This step involves the collection and examination of tide gauge data from multiple stations distributed along the coastline. The data, spanning several decades, provides empirical evidence of past sea-level trends. By normalising these observations to a common reference year, the study establishes a baseline for understanding long-term sea-level changes. In this historical analysis seasonal variations and irregularities have been highlighted, providing the necessary information for model adjustments.

Bias Correction of Climate Models: Following the historical analysis, three bias correction methods have been used to adjust the outputs of 12 CMIP5 climate models. These methods are:

1. Linear Scaling (LS): Using this method, the model outputs have been adjusted by aligning them with the observed mean values, correcting for systemic biases.

2. Variance Scaling (VS): In addition to mean adjustment, this method also corrects for the variance, ensuring that the spread of model predictions matches the observed data.

3. Quantile Mapping (QM): This advanced technique adjusts the entire distribution of model outputs, correcting for higher-order moments and providing a more nuanced fit to the observed data.

1

Each method's effectiveness is evaluated through a comparative analysis with satellite altimetry data, ensuring the corrected models reflect local conditions. The best correction method is selected based on statistical metrics Mean Absolute Error (MAE) and the Coefficient of Determination (R^2), which assess the alignment between corrected model predictions and observed sea levels.

Future Projections: Using the most effective bias correction method identified, the study then adapts future sea-level projections under two Representative Concentration Pathways (RCPs): SSP 4.5 and SSP 8.5. These scenarios represent different trajectories of greenhouse gas emissions, providing a range of potential future climate conditions. SSP 4.5 is a stabilisation scenario where emissions peak around 2040 and then decline, leading to a moderate increase in global temperatures. In contrast, SSP 8.5 is a high-emission scenario where emissions continue to rise throughout the 21st century, resulting in a significant increase in global temperatures (Lee and Romero, 2023). The projections are refined to a monthly resolution, accounting for seasonal fluctuations observed in the historical data. This approach allows for a detailed understanding of how sea levels may change year-to-year and month-to-month, increasing the reliability and usefulness of the projections for regional planning.

Future land movement scenarios at three locations in the study area are extrapolated by comparing historical land movement at these three locations to seven new locations in the study area. By extrapolating the future land movement scenarios from three to 10 locations, a more nuanced elevation map can be incorporated with the sea level projections.

Integration and Scenario Development: The bias-corrected sea-level projections are combined with the ground deformation scenarios to develop coastal impact scenarios. This approach estimates the combined effects of sea-level rise and land movement. Various future coastal scenarios are constructed, considering different rates of sea-level rise. These scenarios are expressed in terms of confidence intervals, highlighting the range of possible outcomes and their associated probabilities.

1.4. STUDY AREA
In this study, I have focused on the coastal area south of Bangkok, particularly around the mouth of the Chao Phraya River in Samut Prakan province. This region is of significant geographical and economic importance, characterised by diverse topography and varied land use.

1.4.1. TOPOGRAPHY
The topography of the southern Bangkok coastal area is predominantly flat and low-lying, typical of deltaic and estuarine environments. Key topographical features include alluvial plains, which are fertile plains formed by alluvial deposits from the Chao Phraya River. These plains are mainly used for agriculture. The region extends into tidal flats and mangrove forests near the coastline. The tidal flats mangroves are vital for coastal protection and biodiversity. The borders of the region are characterised by highly urban-
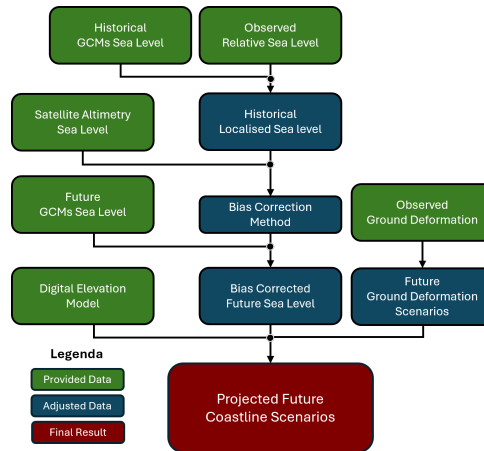
Figure 1.1: Research methodology workflow

ised areas near the river's mouth with significant infrastructure and dense populations (Figure 1.2).

1.4.2. LAND USE

Land use in the coastal area of Samut Prakan is diverse, reflecting the interplay between natural systems and human activities. Agricultural land is prominent, with rice paddies, fruit orchards, and aquaculture thriving due to the region's fertile soils and ample water supply. Urban and industrial development is also substantial, driven by the proximity to Bangkok's central business district. Additionally, the area supports a vibrant fishing and aquaculture industry, characterised by fish farms, shrimp ponds, and traditional fishing communities. Designated mangrove conservation areas provide critical ecosystem services, underscoring the importance of environmental preservation. Moreover, coastal areas have been developed for tourism, featuring beaches and resorts that cater to recreational and tourism activities.

1.4.3. GROUND DEFORMATION IN SAMUT PRAKAN

The diverse land use and unique topography of the coastal area in Samut Prakan present several challenges, particularly as a result of ground deformation. The region has seen extensive groundwater extraction since the mid-20th century, driven by swift urbanisation and industrial growth. Initially, groundwater was tapped as a major source for the population and industrial sector starting around 1954. Leading up to 2010, extraction rates have varied significantly (Figure 1.3).

The excessive withdrawal of groundwater has led to significant land subsidence. The subsidence was particularly noticeable during the 1980s when subsidence rates reached up to 12 cm per year in some areas of Bangkok. This subsidence was mainly due to the compaction of highly compressible alluvial sediments that underlie the city. The geological composition of Bangkok's geological environment includes alternating layers of sand, clay, and peat, with the clay layers being particularly volatile to compaction
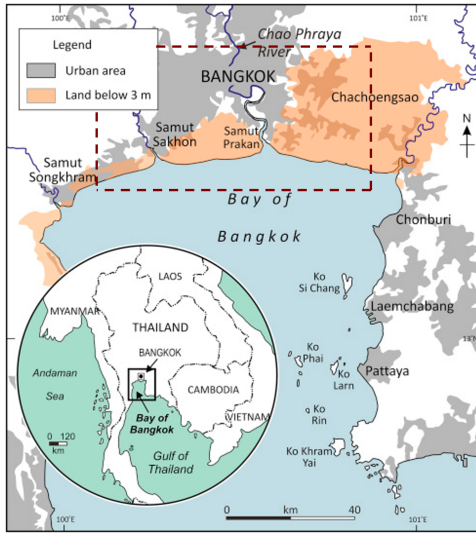
Figure 1.2: Bay of Bangkok with Bangkok, other urban areas and low-lying coastal areas. The study area marked with the red box (Terry et al., 2015).

under stress from decreased pore water pressure. In response to the alarming rates of subsidence and its associated risks—such as increased flooding, infrastructural damage, and saltwater intrusion—the Thai government implemented regulatory measures in the 1980s. These measures aimed to control and reduce groundwater extraction through the establishment of controlled areas where groundwater drilling was restricted and the introduction of higher fees for groundwater use. Despite these efforts, subsidence has continued, although at reduced rates of about 1 cm per year in recent decades, indicating a delayed response of the subsurface system to changes in groundwater levels.

1.5. Thesis Structure

This thesis is organised into seven chapters, each addressing different aspects of the research.

Chapter 2: Literature Review   Chapter 2 provides a review of existing literature on sea-level rise and land subsidence. It examines global and regional studies, highlighting gaps in current knowledge and the need for localised projections in the Gulf of Thailand. This chapter sets the foundation for the research by positioning the study within the broader scientific environment.

Chapter 3: Data   In Chapter 3, I describe the various datasets used in this study. This includes sea-level data from tide gauge observations, historical and future sea-level projections from global climate models, and ground deformation data. The chapter details the sources, characteristics, and preprocessing steps for each dataset.
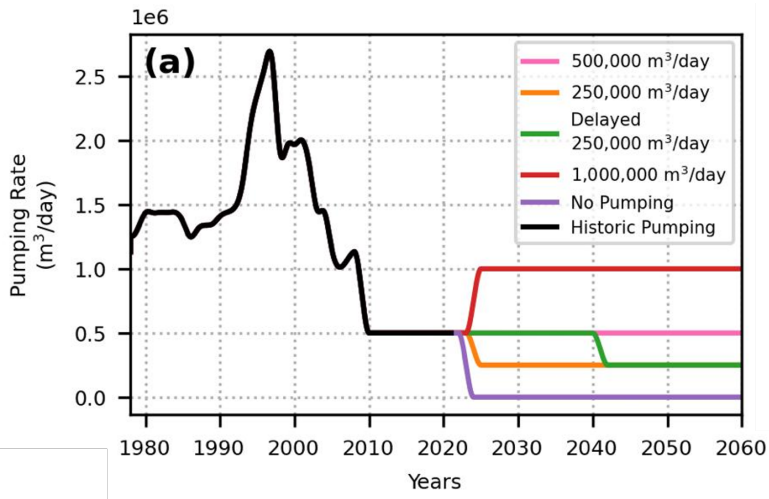
Figure 1.3: Historical water extraction rates in the regulated area encompassing Bangkok and the surrounding seven provinces (black line) and potential future extraction rate from Soonthornrangsan et al., 2023 (coloured lines).

Chapter 4: Methodology   Chapter 4 outlines the methodological framework employed in this study. It begins with the correction of historical GCM outputs using bias the correction methods Linear Scaling, Variance Scaling and Quantile Mapping. This chapter also describes the combination of sea-level forecasts with a DEM. This DEM is adjusted for land subsidence scenarios to develop future coastline scenarios. Detailed steps and equations are provided to ensure transparency and reproducibility.

Chapter 5: Results   In Chapter 5, I present the results of the bias correction methods and the future sea-level projections. This chapter includes statistical analyses comparing corrected model outputs with observed data, as well as visual representations of projected sea-level changes under different emission scenarios. The results are discussed in the context of their implications for coastal vulnerability in the Gulf of Thailand.

Chapter 6: Discussion   Chapter 7 delves into the broader implications of the findings, exploring potential future research directions and the practical applications of the study. It discusses the limitations of the current research and suggests ways to address these in future studies. Additionally, this chapter examines the policy implications of the projections for coastal management and climate adaptation in the Gulf of Thailand.

Chapter 7: Conclusion   The research question and sub-questions have been answered in Chapter 6. By answering these questions the key findings of the research are combined, highlighting the contributions of the study to the existing body of knowledge.

2

LITERATURE REVIEW

Understanding SLR and land deformation in the Gulf of Thailand, and particularly in the northern regions of the Gulf, is critical due to the highly populated, low-lying coastal areas. In this chapter, I provide a comprehensive overview of existing research on global and regional sea-level rise trends and the mechanisms and impacts of land subsidence. I explore the interaction between sea-level rise and land subsidence, highlighting their compounded effects on coastal vulnerability. Additionally, I cover methodologies for bias correction in climate models to ensure accurate future projections.

GLOBAL AND REGIONAL SLR DYNAMICS

Global studies, such as those by Nerem et al. (2022), show that the rate of global mean sea-level rise has increased from about 1.7 mm/year in the 20th century to around 3.3 mm/year since 1993. Palmer et al. (2021) offer a comprehensive overview of recent advancements in understanding global mean sea level changes. The current consensus estimate, as outlined in Chapter 9.6.1 of the IPCC AR6 Working Group I report (Fox-Kemper et al., 2023), indicates an accelerated rise in global mean sea levels. This research shows the critical role of historical data in understanding long-term trends.

These global perspectives provide valuable insights but lack the detailed information needed for regional applications. For example, the Gulf of Thailand experiences unique local phenomena that can differ significantly from global trends. Trisirisatayawong et al. (2011) highlighted the impact of vertical land motion on SLR in the Gulf of Thailand but did not integrate these local insights into broader climate models, which is essential for accurate future forecasts.

ADVANCED TECHNOLOGIES AND BIAS CORRECTION IN REGIONAL ANALYSIS

Regional studies, like those by Tebakari (2020), use high-resolution elevation data to assess vulnerabilities in the Bangkok metropolitan area to SLR. Tebakari's approach demonstrates the usefulness of precise elevation data in evaluating flood risks and planning urban adaptations to future sea-level scenarios. However, Tebakari's study does not integrate these findings into predictive climate models that can forecast long-term changes under various greenhouse gas emission scenarios.

Phien-wej, Giao, and Nutalaya (2006) highlighted land subsidence in Bangkok, showing that subsidence rates can reach up to 10 mm/year in some areas. This significantly affects relative sea-level measurements and necessitates local adjustments to global SLR data.

Soonthornrangsan et al. (2023) expanded on this by introducing a hybrid data-driven and physics-based approach to simulate land subsidence caused by groundwater pumping. Their study focused on Bangkok, demonstrating the potential of this approach even with sparse data. They found that land subsidence in Bangkok is significantly influenced by groundwater extraction, with the model accurately simulating subsidence despite data limitations. This research supports the necessity of incorporating subsidence data into SLR models to improve the accuracy of regional projections.

Accurate regional projections require adjustments to climate models by tide gauge and satellite data to reflect true sea-level changes, as discussed by Dean (2013) and Wahl (2013). These adjustments vary significantly between regions and must be validated against local conditions.

Expanding on these technical adjustments, Palmer et al. (2020) discuss advanced statistical methods to localise sea-level data, introducing techniques like Quantile Mapping and Variance Scaling, which are crucial for reducing prediction uncertainties in regional models. These methods refine the raw data to better match observed historical patterns, addressing discrepancies found in earlier models.

LOCAL IMPACTS, ADAPTATION STRATEGIES, AND FUTURE PROJECTIONS

Jaroenongard (2021) applied the correction methods to the Gulf of Thailand, highlighting the significant differences between sea level predictions from GCM and actual local sea levels. However, Jaroenongard does not combine the SLR projections with coastal digital elevation models to show the increasing vulnerabilities of coastal populations. This integration is essential for mitigation planning in the Gulf of Thailand. Phien-wej et al. (2006) documented significant subsidence rates in Bangkok, exacerbating the impacts of rising sea levels. Soonthornrangsan et al. (2023) further emphasised that integrating groundwater modeling with subsidence data is critical for accurate SLR projections.

This research adresses the gap in the literature where localised SLR forecasts are combined with a digital elevation model, which is adjusted for land subsidence. The proposed research integrates high-resolution topographic data with refined bias correction methods applied to CMIP5 model outputs. This will provide detailed projections of SLR under SSP 4.5 and SSP 8.5 scenarios, localised for the Gulf of Thailand. By combining localised SLR forecasts with potential future ground elevation, a better understanding of future coastline scenarios could be accomplished. Such a better understanding could offer actionable insights for policymakers and coastal managers, aiding in the development of more effective adaptation and mitigation strategies.

3

SEA-LEVEL DATA COLLECTION AND PROCESSING

The data required for the study consist of four sea-level data sets in the Gulf of Thailand (GoT) and ground deformation scenarios for the coastal regions adjacent to the GoT. The four sea-level data sets are (i) observed relative sea-level data at tide gauge stations in the GoT, (ii) historical regional sea-level projections provided by Global Climate Models (GCMs), part of the Coupled Model Intercomparison Project Phase 5 (CMIP5) and (iii) future regional sea-level projections provided by the Intergovernmental Panel on Climate Change (IPCC), (iv) satellite sea-level altimetry data from the Copernicus Mission. The satellite altimetry data is used for the verification of the adjusted CMIP5 models. The ground deformation scenarios have been provided by (Soonthornrangsan et al., 2023).

3.1. SEA LEVEL DATA

To understand SLR in the Gulf of Thailand, it is essential to analyze various sea-level datasets. This section describes the collection and characteristics of observed relative sea-level data from tide gauge stations, historical sea-level projections from GCMs, satellite altimetry data from Copernicus Climate Change Service (C3S) and future projections from the IPCC. These datasets provide a foundation for assessing sea-level changes in the region.

3.1.1. TIDE GAUGE OBSERVATIONS

Sea-level observations were retrieved from the Permanent Service for Mean Sea Level (PSMSL) database for five selected tide gauge stations: Ko Sichang, Phra Chulachomaklao Fort, Ko Lak, Ko Mattaphon, and Geting. The geographical locations of these stations are spread throughout the coastline of the GoT and have been illustrated in Figure 3.3b.

For each station, sea-level readings are anchored to a Revised Local Reference (RLR). This RLR is different for each station, making it necessary to normalise the data to facilitate inter-station comparisons. This normalisation involved adjusting the data to reflect
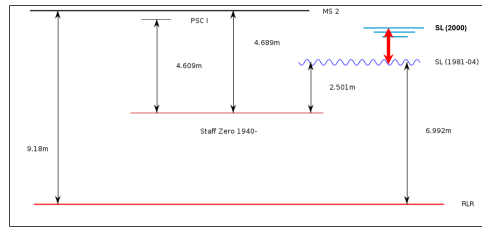
Figure 3.1: Visual representation of the reference frame containing the tide gauge sea level measurements as the blue waving line relative to the red RLR and the mean sea level in the year 2000 as the flat blue line.

sea-level change relative to the mean recorded levels in the year 2000 at each respective station, thus enabling the analysis of relative sea-level changes among the stations (Figure 3.1).

Data from Phra Chulachomklao Fort were excluded from the analysis due to significant distortion from land subsidence linked to groundwater extraction.

Monthly tide gauge data for the remaining four stations are displayed in Figure 3.2a. The observation periods vary, with Ko Lak providing the longest dataset from 1940 to 2022, followed by Ko Sichang (1940-2002), Geting (1987-2017), and Ko Mattaphon (1993-2022) (Holgate et al., 2013).

The data collected at Ko Lak shows a relatively consistent increase in sea level with an estimated slope of 1.45 mm/year. This indicates a gradual sea level rise over the period observed. The spread of data points around the trend line is fairly uniform, suggesting minor intra-annual and inter-annual variability compared to long-term trends.

The measurements at the station in Ko Sichang show a more subtle increase in sea level, with a slope of 0.74 mm/year. The spread of data points is wider than in Ko Lak, which may indicate greater variability or less stability in sea level measurements at this location.

The sea level trend in Geting is more pronounced, with a steeper increase in sea level at a rate of 3.34 mm/year. This station shows a higher rise compared to Ko Lak and Ko Sichang.

The station in Ko Mattaphon has the highest rate of increase among the four, with a slope of 4.79 mm/year. The consistent upward trend and relatively tight clustering of data points around the trend line indicate a strong, steady rise in sea level.

The gaps in data, noticeable in certain periods across the stations (for example, Ko Mattaphon in 2005 and Ko Sichang in the first half of 2001), could be due to issues with data collection methods, maintenance of tide gauge equipment, or external events that disrupted measurements.

Figure 3.2b presents the monthly sea level data for the four operational stations, normalised to the 2000 mean, covering the period from 1988 to 2002. These sea-level observations reveal a consistent seasonal pattern, with higher sea levels observed in winter and lower levels in summer.

Details of the tide gauge stations and sea-level observations are depicted in table 3.1.
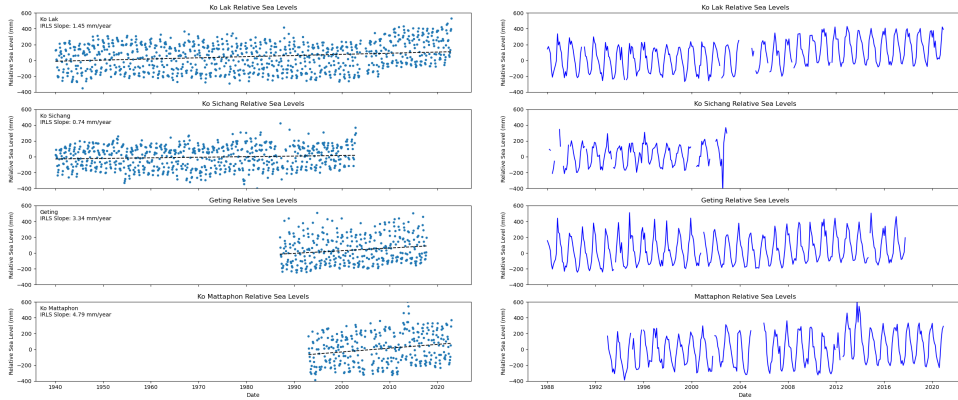
(a) Observations between 1940 and 2022 (b) Observations between 1988 and 2020

Figure 3.2: Monthly sea level observations at the four tide gauge stations in the Gulf of Thailand relative to the mean sea level in 2000

Table 3.1: Details of tide gauge stations and observed sea-levels used in this study (Holgate et al., 2013)

Station	Location		Frequency	Data Period	Remarks
	Lat	Lon			
Ko Sichang (KS)	13° 09' 00" N	100° 49' 00" E	Monthly	1940-2002	Data missing for 2000 and 2001
Ko Lak (KL)	11° 48' 00" N	99° 49' 00" E	Monthly	1940-2022	Data missing for 2004
Ko Mattaphon (KM)	10° 26' 60" N	99° 15' 00" E	Monthly	1993-2022	Data missing for 2005
Geting (Ge)	6° 13' 33" N	102° 06' 22" E	Monthly	1987-2017	

3.1.2. HISTORICAL GCMS SEA-LEVELS

Section 4.1 Historical GCM Correction incorporates historical sea-level simulations provided by the Netherlands Institute for Sea Research (NIOZ). These simulations are derived from a suite of twelve climate models, part of the fifth phase of the Climate Model Intercomparison Project (CMIP5). Details of the 12 climate models can be seen in table 3.2. As an example, we show sea-level simulations for four models at 10.5°N; 100.5°E, one of the 11 locations at which the models provide data in the GoT (Figure 3.3). All simulations have been normalised to the simulated mean sea-level of the year 2000 for each model separately to allow for comparison.

All the listed models are coupled climate models, meaning they integrate various components of the Earth system, such as the atmosphere, ocean, land surface, and sea ice, to simulate climate dynamics. Each of these models participated in the Coupled Model Intercomparison Project Phase 5 (CMIP5), contributing to the IPCC Fifth Assessment Report (AR5) and provide global climate simulations and projections, allowing for analysis of large-scale climate patterns and changes across the entire planet.

The models vary in their horizontal atmospheric resolutions. For instance, CCSM4 has a finer resolution (0.94° x 1.25°) compared to CanESM2 (2.81° x 2.81°), which affects the detail and accuracy of their simulations. Different models excel in simulating various climate features. For example, while CCSM4 and GFDL-CM3 are noted for their improved representation of ENSO variability (Gent et al., 2011) (Delworth et al., 2006), the

HadGEM2-ES model is recognised for its advanced simulation of the hydrological cycle, including more accurate precipitation patterns and extreme weather events (Collins et al., 2011).
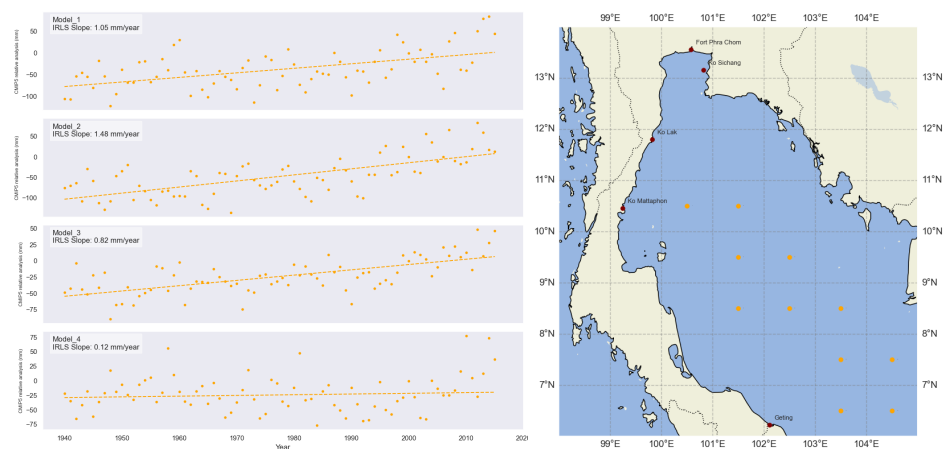
(a) Yearly historical sea-level simulations relative to the year 2000, model 1-4 at latitude 10.5°N and longitude 100.5°E

(b) Tide gauge stations (red) and climate model locations (orange)

Figure 3.3: Comparison of sea-level predictions and model locations

Table 3.2: Ensemble of 12 CMIP5 climate models used to estimate the twentieth-century sea-level rise

Model ID	Institute, country	Atmosphere Grid Lat° x Lon°	Ocean Grid Lat° x Lon°	Main Reference
1. CanESM2	CCCma, Canada	2.81 x 2.81	0.94 x 1.40	Arora et al., 2011
2. CCSM4	NCAR, USA	0.94 x 1.25	0.47 x 1.12	Gent et al., 2011
3. CNRM-CM5	CNRM-CERFACS, France	1.41 x 1.41	0.62 x 0.99	Voldoire et al., 2013
4. GFDL-CM3	NOAA GFDL, USA	2.00 x 2.50	0.90 x 1.00	Delworth et al., 2006
5. GISS-E2-R	NASA GISS, USA	2.00 x 2.50	1.00 x 1.25	Schmidt et al., 2006
6. HadGEM2-ES	MOHC, UK	1.24 x 1.87	0.83 x 1.00	Collins et al., 2011
7. IPSL-CM5A-LR	IPSL, France	1.87 x 3.75	1.21 x 1.98	Dufresne et al., 2013
8. MIROC5	MIROC, Japan	1.41 x 1.41	0.80 x 1.41	Watanabe et al., 2010
9. MIROC-ESM	MIROC, Japan	2.81 x 2.81	0.94 x 1.41	Watanabe et al., 2011
10. MPI-ESM-LR	MPI-M, Germany	1.88 x 1.88	0.82 x 1.41	Stevens et al., 2013
11. MRI-CGCM3	MRI, Japan	1.12 x 1.12	0.49 x 1.00	Yukimoto et al., 2012
12. NorESM1-M	NCC, Norway	1.88 x 2.50	0.47 x 1.12	Tjiputra et al., 2013

3.1.3. FUTURE SEA-LEVEL PROJECTIONS

To forecast future sea-level changes in the Gulf of Thailand, I use regional sea-level projections from the Sixth Assessment Report (AR6) of the Intergovernmental Panel on Climate Change (IPCC) (Fox-Kemper et al., 2023). The AR6 report includes updated sea-

level projections under various greenhouse gas concentration trajectories, with SSP4.5 and SSP8.5 serving as the primary scenarios for this research (O'Neill et al., 2014).

SCENARIO SSP4.5

The SSP4.5 scenario represents a moderate mitigation pathway where global warming is likely to stabilize at approximately 2.4°C above pre-industrial levels by the end of the 21st century. Under this scenario, the IPCC AR6 projects a median sea-level rise of approximately 0.52 meters relative to the 1995-2014 average by the year 2100. The projections account for contributions from thermal expansion, glacier melt, and polar ice sheet dynamics. This scenario is critical for assessing potential coastal impacts under relatively optimistic emission reductions (Lee and Romero, 2023).

SCENARIO SSP8.5

In contrast, the SSP8.5 scenario assumes continued high emissions leading to a significant increase in global temperatures, approximately 4.4°C above pre-industrial levels by 2100. Under this scenario, the projected median sea-level rise is about 0.84 meters by the end of the century. SSP8.5 represents a high-risk scenario that is vital for planning under worst-case climate conditions (Lee and Romero, 2023).

The projections for both emission scenarios are presented as three confidence scenarios to illustrate the uncertainties inherent in climate modelling, namely the 5%, 50% and 95% confidence interval (Figures 3.4a and 3.4b), where the 50% confidence interval is the median of the range of predictions.

(a) Scenario SSP2-45   (b) Scenario SSP5-85
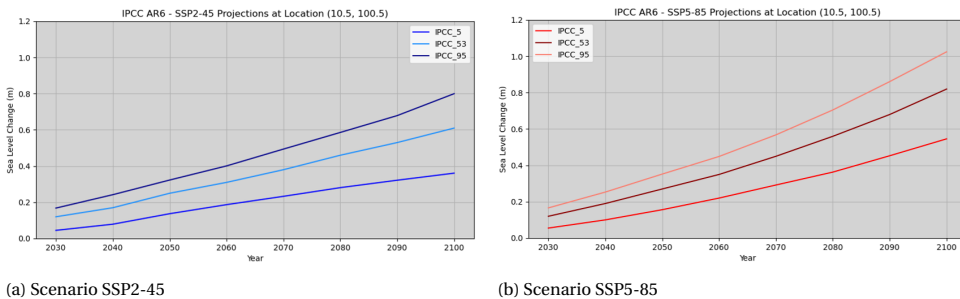
Figure 3.4: Yearly sea-level change projections from the IPCC AR6 report for both emission scenarios at latitude 10.5°N and longitude 100.5°E. Confidence intervals 5%, 50% and 95%

3.1.4. VALIDATION DATA: COPERNICUS ALTIMETRY DATA

For the validation of the sea-level model adjustments, this study uses satellite sea-level observations from the Copernicus Climate Change Service (C3S), specifically the "Satellite Sea Level Global" dataset (Copernicus Climate Change Service, 2018). This dataset provides high-resolution, gridded sea-level data from 1993 to the present, derived from a series of satellite altimetry missions. The dataset's comprehensive temporal coverage and consistent quality make it an invaluable resource for assessing the accuracy of sea-

level projections.

The C3S sea level altimeter product relies on a stable satellite constellation to ensure long-term ocean observation stability. It covers the period from January 1993 until a few months before the present time (August 2024). It includes reference missions, complementary missions, and missions of opportunity:

Reference Missions: These are essential for computing the long-term trend of mean sea level (MSL). They include TOPEX/Poseidon, Jason-1, Jason-2, Jason-3, and Sentinel-6MF, with Sentinel-6MF replacing Jason-3 in February 2022.

Complementary Missions: These provide additional data for estimating mesoscale signal variabilities and enhance observing capacity at high latitudes. Missions include ERS-1, ERS-2, Envisat, SARAL/Altika, and currently, Sentinel-3A.

Missions of Opportunity: After the loss of Envisat in April 2012, CryoSat-2 was included until SARAL/AltiKa data became available in March 2013.

It's important to note that reference and complementary missions are distinct concepts in the C3S product. While coverage refers to the overall spatial and temporal extent of the sea level data, complementary missions are specific satellite missions used to enhance this coverage, particularly for estimating mesoscale variabilities and improving observations at high latitudes. These complementary missions also play a important role in maintaining data continuity when gaps occur in the primary mission data.

The dataset offers global coverage with a spatial resolution of approximately 0.25 degrees, providing detailed insights into sea-level changes. It includes corrections for various factors such as atmospheric pressure, tides, and sea state bias, ensuring high accuracy and reliability of the measurements. The altimetry satellite constellation used in the C3S sea level product is illustrated in Figure 3.5 (Copernicus Climate Change Service, 2018), where as the altimetry tracks from the Topex/Jason and the Envisat missions can be seen to cover the Gulf of Thailand profoundly (Figure **??**.
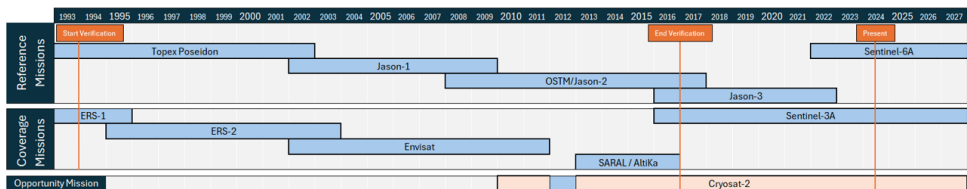
Figure 3.5: Satellite constellation in the C3S time series.

3.2. GROUND DEFORMATION DATA

Ground deformation, particularly land subsidence, is a significant factor affecting the coastal regions in Samat Prakan, magnifying the impacts of sea-level rise. This section

Figure 3.6: Two of the ground tracks of altimetry satellites, Topex/Jason and Envisat, used in the verification of the adjusted models in this research. The locations of the four tide gauge station can be seen among the blue dots (Trisirisatayawong et al., 2011).

discusses the sources and methods of data collection related to ground deformation used in this research.

3.2.1. COASTAL DIGITAL ELEVATION MODEL

For this research, the CoastalDEM v2.1 is used as the primary Digital Elevation Model (DEM). CoastalDEM v2.1 is a high-accuracy and high-resolution global coastal digital elevation model developed by Climate Central. CoastalDEM v2.1 was created to improve upon previous global elevation models, particularly for assessing coastal vulnerability to sea level rise and flooding. The DEM is based on data from NASA's ICESat-2 satellite mission, which was launched in 2018 (Kulp and Strauss, 2023).

SATELLITE MISSION: ICESAT-2

The ICESat-2 mission provides high-precision elevation measurements using satellite lidar technology. Unlike its predecessor, ICESat, which operated from 2003 to 2010 and had limitations in data density and accuracy, ICESat-2 offers more frequent and accurate measurements. The satellite uses six laser beams, arranged in three pairs, spaced 3 kilometres apart, and provides elevation values every 100 meters along its track. These measurements allow for precise elevation data even in densely vegetated or urban areas.

BIAS AND ACCURACY

CoastalDEM v2.1 significantly reduces the vertical bias and root mean square error (RMSE) present in earlier models like NASA's Shuttle Radar Topography Mission (SRTM). The

ICESat-2 data used for training the model contains a vertical bias of less than 10 centimetres and an RMSE of less than 1 meter, making it highly reliable for coastal elevation assessments. In global evaluations, CoastalDEM v2.1 exhibits a median vertical bias close to zero and outperforms other leading global DEMs in low-lying and densely populated areas, which are critical for coastal vulnerability assessments. The DEM can be seen in Figure 3.7.

To further verify the accuracy of CoastalDEM v2.1, I compared the DEM's coastline location with high-resolution Google Earth imagery captured during different seasons. Figures 3.8b and 3.8a show Google Earth snapshots of the coastline and sea level in June 2022 and October 2022, respectively. These images were chosen to represent the variability in sea levels between summer and winter. As illustrated in these figures, the DEM coastline (visualised as the red line) consistently lies between the high water levels observed in winter (October) and the low water levels in summer (June). In Figure 3.8b, the sea has pulled back all the way

The temple seen in both images is completely surrounded by water in Figure 3.8a due to the high sea level. In Figure 3.8b, the sea has retreated to the bottom of the image. This can be deduced from the fact that in Figure 3.8b the grooves in the seabed can be seen.

This positioning confirms that CoastalDEM v2.1 accurately captures the general location of the coastline, taking into account the seasonal variability of sea levels.
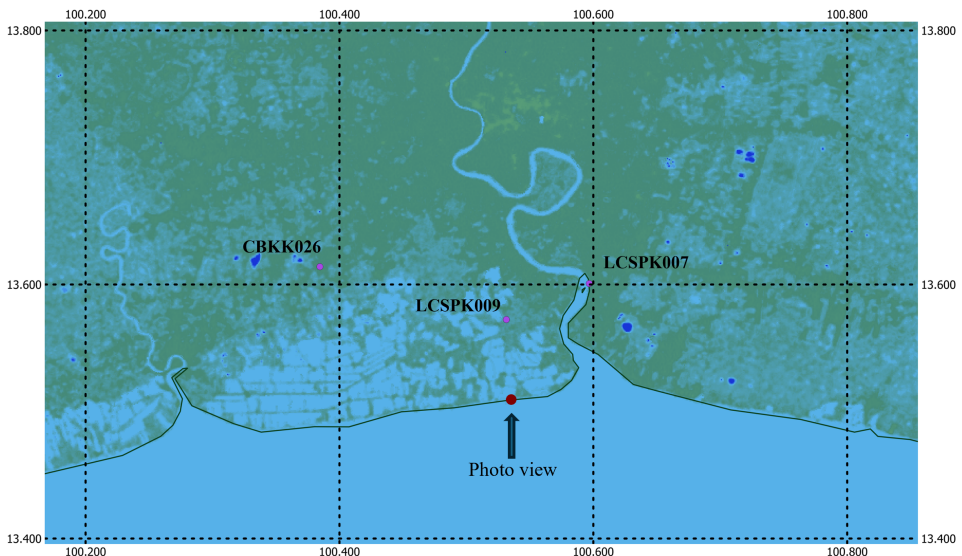
Figure 3.7: CoastalDEM v2.1 in 2021 with the land deformation locations provided by Soonthornrangsan et al., 2023 and the location of the Google Earth snapshots represented as the red dot.

(a) Sea level and coastline in October 2022   (b) Sea level and coastline in June 2022

Figure 3.8: Coastline and sea-level representation during October and June in 2022 accompanied by the coast-line from the CoastalDEM v2.1 visualised as the red line.

3.2.2. FUTURE SUBSIDENCE SCENARIOS

Using a data-driven and physics-based modeling approach, Soonthornrangsan et al. (2023) provided ground deformation forecasts for three locations in Bangkok and Samut Prakan from 2020 to 2100, namely LCBKK026, LCSPK007, and LCSPK009 (Figure 3.7). Based on the provided forecasts, continuing subsidence through the 21st century is expected at these three locations, although at varying rates. The projections provided by Soonthornrangsan et al., 2023 are presented in Figure 3.9. These projections are integrated with localised SLR forecasts, obtained from the AR6 report of the IPCC, to assess future coastline scenarios. This step will be covered in Section 4.5.
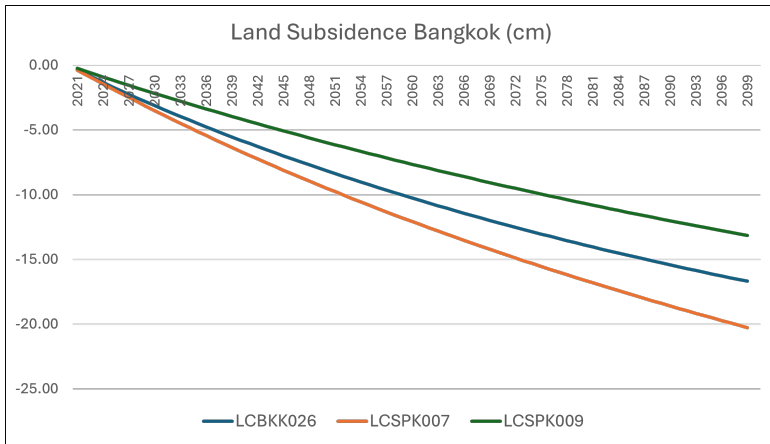
Figure 3.9: Land subsidence scenario for locations LCBKK026, LCSPK007, and LCSPK009 provide by Soonthornrangsan et al., 2023 between 2021 and 2100.

4

BIAS-CORRECTION AND LOCAL REFINEMENT OF SEA-LEVEL ESTIMATES

To forecast the future configuration of Samut Prakan's coastline, in this study two main factors contributing to coastal progression have been investigated: sea-level rise and land subsidence. Based on these two factors, coastline scenarios in the year 2100 have been developed.

A critical aspect of the study involves comparing historical local sea-level projections, as provided by the CMIP5, with tide gauge observations from four locations in the Gulf of Thailand.

To adjust for discrepancies between the modelled data from CMIP5 and the observed sea-level, three distinct bias correction techniques have been employed: linear scaling, Variance scaling with mean correction, and quantile mapping. Subsequently, the statistical metrics Mean Absolute Error (MAE) and the Coefficient of Determination (R^2) will be used to assess the effectiveness of each bias correction method in aligning the CMIP5 model historical predictions with satellite altimetry observations.

After the best performing bias correction method is chosen, IPCC AR6 future sea-level predictions for both Representative Concentration Pathways (SSP) 4.5 and SSP 8.5 are adjusted based on the calculated correction factors. These projections will be presented as a range, capturing the variability and uncertainties both in the model outputs and the bias correction process. The refined projections, when combined with land subsidence scenarios, will facilitate a range of relative sea-level projections.

Finally, based on these projections, various coastline scenarios have been developed. These scenarios will be instrumental in providing insights into potential impacts on the coastal regions.

4.1. HISTORICAL GCM CORRECTION

Accurate prediction of future sea levels requires precise adjustments to historical GCM outputs to correct inherent biases. In this section the methods used to align historical GCM predictions with observed sea-level data have been outlined, ensuring the models more accurately reflect local conditions and seasonal variations.

4.1.1. SEASONAL FLUCTUATION ADJUSTMENT

The historical CMIP5 models provided by the NIOZ contain yearly data points, which are very helpfull for understanding long-term sea-level trends. However, to be able to scale the CMIP5 predictions with the monthly tide gauge measurements, the yearly sea-level analysis from CMIP5 have to be extrapolated to represent monthly sea-level values. The intra-annual fluctuations in tide gauge data have been used to extrapolate these yearly predictions to monthly predictions. This adjustment accounts for the prominent seasonal sea-level variations driven primarily by monsoon impacts, which are well-documented in the region. Studies such as Saramul (2017) which used high-frequency radar to study the fluctuations have emphasised that the monsoon winds significantly influence these fluctuations, with higher sea-levels typically observed during the northeast monsoon in winter and lower levels during the southwest monsoon in summer. The average fluctuation factors at each tide gauge station can be found in figure B.1 in Appendix B.

To integrate the monthly variation into the CMIP5 sea-level analysis, tide gauge readings were organised annually to calculate the average sea level for each year. Then, the monthly deviation from this annual average was determined. This approach helps in calculating a fluctuation factor for each month by averaging the deviations noted in the same month across different years—for instance, averaging all January deviations over the recorded period to derive the January fluctuation factor. This factor is essential for adjusting yearly CMIP5 model data to monthly data, before the data is scaled by the tide gauge observations.

The adjusted sea-level predictions for month m in year y are thus calculated using the equation (4.1).

$$M_{\text{adjusted},m,y} = M_y \times F_m,\tag{4.1}$$

where M_y are the annual model predictions from each of the 12 CMIP5 models, and F_m denotes the fluctuation factor for month m. This approach ensures that our model predictions are now suited to be scaled by the tide gauge measurements. The sea-level analysis from Model 1 between the year 2000 and 2016, extrapolated based on the mean monthly fluctuations are presented in Figure 4.1a.

4.1.2. BIAS CORRECTION METHODS

The extrapolated CMIP5 dataset provides coarse-scaled climate and sea-level information that needs refining to a more detailed scale for local analysis. I used Bias-correction methods to fine-tune the raw extapolated CMIP5 data, localising the climate model sea level analysis to the Gulf of Thailand. This study I have assessed three methods to sharpen CMIP5 sea-levels data from 1940-2021, namely linear scaling (LS), mean variance scal-

ing (VS), and quantile mapping (QM). The most reliable method will be used to extend future SLR along the coast of the Gulf of Thailand.

Firstly, linear scaling is used to refine the extrapolated sea-level data, adjusting it to align with actual observations. Linear scaling is one of the simplest bias correction methods. The mean on the model outputs is aligned with observations, therefor addressing mean biases which are often present in climate models. When models are linearly scaled, the central tendency of the model outputs is matched with the observed data. The effectiveness of linear scaling in precipitation and temperature data is demonstrated by Teutschbein and Seibert, 2012. Equation (4.2) shows the method used for linear scaling.

$$SL_{cor, \text{m, yr}} = SL_{\text{raw, m, yr}} + \mu\left(SL_{obs, \text{m}}\right) - \mu\left(SL_{\text{raw, m}}\right), \tag{4.2}$$

where SL refers to the sea-level, μ refers to mean value, *cor* refers to the corrected value, *raw* refers to raw data, and *obs* refers to the corrected tide gauge data.

Secondly, the Variance Scaling method corrects both the mean and the variance of time series. This method ensures the spread of the predictions matches the observations. Not only biases in the central tendency are addressed, but also the variability of the model outputs. The distribution of the model predictions is adjusted to better match the observed variability. Teutschbein and Seibert, 2012 applied variance scaling to improve the representation of temperate and precipitation in climate models. The sea level prediction is corrected using equation (4.3).

$$SL_{cor, \text{m, yr}} = \left(\left[SL_{\text{raw, m, yr}} - \mu\left(SL_{\text{raw, m, yr}}\right)\right] \times \frac{\sigma\left(SL_{\text{obs,, m}}\right)}{\sigma\left(SL_{\text{raw, m}}\right)}\right) + \mu\left(SL_{obs, \text{m, yr}}\right), \tag{4.3}$$

where SL refers to the sea-level, μ refers to mean value, σ refers to variance, *cor* refers to the corrected value, *raw* refers to raw data, and *obs* refers to corrected tide gauge data.

Quantile mapping is a bias correction method that adjusts the entire distribution of model predictions. The method provides a more balanced fit to the observed data by correcting the mean, the variance and higher-order moments of distribution. quantile mapping has the ability to correct complex biases in climate model outputs. This method can be applied when biases in extremes and tails of distributions have be to taken into account. The effectiveness of quantile mapping is shown by Cannon et al., 2015 when biases in temperature and precipitation extremes have to be minimised in climate models. The quantile mapping method is denoted in equation (4.4).

$$SL_{(cor), \text{ year}} = F_{\text{obs}}^{-1}\left(F_{CMIP5}\left(SL_{(\text{raw}), \text{ year}}\right)\right), \tag{4.4}$$

where SL refers to the sea-level, *cor* refers to the corrected value, *raw* refers to raw CMIP5 data, and *obs* refers to corrected tide gauge data. F_{obs}^{-1} is the inverse quantile function corresponding to the corrected tide gauge observation and F_{CMIP5} is the quantile function corresponding to the CMIP5 output.

DISTANCE DETERMINATION VIA THE HAVERSINE EQUATION AND SPATIAL INTEGRATION
In this study, sea-level re-analysis predictions from 12 CMIP5 models for 11 specific locations in the Gulf of Thailand were adjusted based on data from four tide gauge stations. By adjusting model predictions with real-world observations, I aim to ensure that the model predictions more accurately reflect local sea-level variations. For each location, predictions from each CMIP5 model were scaled by the observations from each tide gauge station, resulting in four distinct scaled models per location, per CMIP5 dataset. These scaled models were then combined into a singular analytical model per location for each CMIP5 dataset. The combination was based on the spatial distances between the model locations and the tide gauge stations to accurately integrate spatial relationships.

The calculation of these distances was conducted using the Haversine equation, a trigonometric method designed to estimate the shortest path between two points on a spherical surface based on their latitudes and longitudes. Haversine distance determination is chosen for this study because it provides an accurate method to calculate the shortest distance between two points on a spherical surface. The Earth's curvature is taken into account, making it suitable for geographical use where precise distance measurements are critical. The equation guarantees that the spatial weighting of model outputs is based on accurate distances between tide gauge stations and prediction locations. By using this method the reliability of the adjusted projections is improved. According to Sinnott (1984), the Haversine equation is widely used in geospatial analysis due to its effectiveness in calculating distances over the Earth's surface. The Haversine equation is expressed as:

$$D_{ik} = 2r \arcsin\left(\sqrt{\sin^2\left(\frac{\varphi_k - \varphi_i}{2}\right) + \cos\varphi_i \cdot \cos\varphi_k \cdot \sin^2\left(\frac{\lambda_k - \lambda_i}{2}\right)}\right) \qquad (4.5)$$

In this equation, D is the distance between two points, r is the Earth's radius (approximated as 6,371 kilometers), ϕ_i, ϕ_k denote the latitudinal coordinates in radians and λ_i, λ_k the longitudinal coordinates in radians of the two points, respectively.

Following the computation of distances between the climate modeling sites and tide gauge stations, as documented in Table A.1, these distances were utilised to derive a weighting factor for combining the scaled models. The scaled model outputs, each representing a unique pairing of a climate model with a tide gauge observation, were adjusted by their respective weighting factors. The weighting factor W_{ij} for the jth model at the ith location is inversely proportional to the distance D_{ik} and is normalised by the sum of the inverses of all distances for the location:

$$W_{ij} = \frac{\frac{1}{D_{ik}^P}}{\sum_{k=0}^{4} \frac{1}{D_{ik}{}^P}} \qquad (4.6)$$

where P is a power parameter that adjusted the sensitivity of the weight to the distance, and k indexes the four tide gauge stations. The computed weight factors based on the distances and a power parameter $P = 2$ are detailed in the Table A.2

The combined model output C_i for the ith location is then calculated as a weighted sum of the model outputs, using the weight factor W_{ij}:

$$C_i = \sum_{j=1}^{4} W_{ij} \cdot M_{ij} \tag{4.7}$$

This equation ensures that each model's contribution to the final combined output is weighted by its relative distance to the tide gauge station, as determined by the distance D_{ij} and the calculated weight factor W_{ij}. This approach allows for a balanced combination of the models, taking into account the spatial relationships between the locations and the tide gauge stations, thereby enhancing the precision and relevance of the CMIP5 model predictions in relation to the observed sea-level data from the tide gauge stations in the Gulf of Thailand.
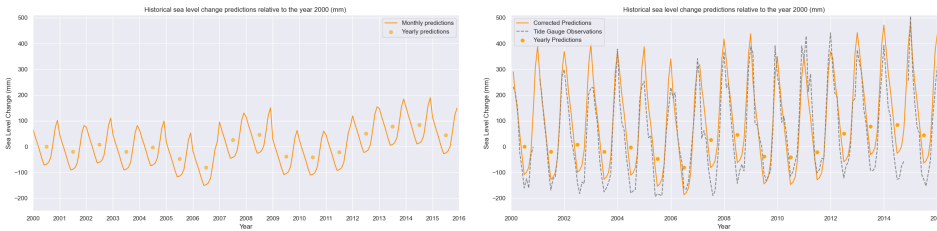
(a) Extrapolated to monthly sea level analysis.

(b) Extrapolated and corrected sea level analysis.

Figure 4.1: Yearly Historical sea-level predictions from Model 1 from CMIP5. Extrapolated to monthly values by fluctuation factors based on the seasonal sea-level change and corrected by sea level measurements at the Geting tide gauge station.

4.2. PERFORMANCE STATISTICS

Two performance statistics have been used to evaluate the correction-bias methods. Namely the Mean Absolute Error (MAE), with a desired value of 0 and the Coefficient of Determination (R^2), with a desired value of 1. The MEA and the R^2 values represent the correlation between the corrected model predictions and the satellite altimetry sea-level change.

The Mean Average Error (MAE) is chosen as a performance metric for multiple reasons. The MAE is straightforward to interpret as it represents the average absolute difference between predicted and observed values. This makes it easier to understand the model's performance in practical terms. In this practice the MAE is used to determine the average error in millimetres when predicting sea levels. Secondly, unlike metrics that square the errors (such as Mean Squared Error), MAE treats all errors equally. This characteristic is useful when large errors should not be excessively penalised, maintaining a balanced view of model performance across all prediction errors. Lastly, the MAE directly measures the accuracy of the model by averaging the absolute errors between the adjusted model outputs and the observed sea levels from the Copernicus Altimetry data.

The Coefficient of Determination (R^2) is the second metric for evaluating the performance of the adjusted model outputs. R^2 provides a measure of how well the observed outcomes are replicated by the model, based on the proportion of total variation of outcomes explained by the model. This is important for validating the reliability of the sea level predictions made by the models. Moreover, using R^2 allows for easy comparison between different models or correction methods. It provides a normalised measure that can quickly indicate which model or method performs better in capturing the relationship between predicted and observed values.

The equations used to calculate the performance statistics are (Jaroenongard et al., 2021):

$$MAE = \frac{1}{n} \sum_{i=1}^{n} |X_i - Y_i|, \tag{4.8}$$

$$R^2 = \left(\frac{\frac{1}{n} \times \sum_{i=1}^{n} \left[(x_i - \bar{x}) \times \left(y_i - \bar{y} \right) \right]}{\sigma_x \times \sigma_y} \right)^2, \tag{4.9}$$

where x_i is observed sea-level for combination month and year i, $\overline{x}$ is the average of observed sea-level, n is number of data points, y_i is simulated sea-level for combination month and year i by the CMIP5 models, $\overline{y}$ is the average of simulated sea-levels, and σ_x and σ_y are the standard deviation of observed and simulated sea-level.

4.3. Future sea-level Projections

This research uses decadal sea-level projections derived from the RCP SSP4.5 and SSP8.5 scenarios, as outlined in the IPCC reports. These scenarios represent varied trajectories of greenhouse gas emissions and their impact on global sea-levels. The IPCC's sea-level forecasts, which account for land deformations, have been adapted by the NIOZ to provide absolute sea-level forecasts without land deformation components. This adaptation enables the integration of the IPCC AR6 sea-level forecasts with local deformation scenarios in Thailand.

Recognising the need for finer temporal resolution, these decadal projections have been interpolated into annual projections, and further refined to monthly projections using fluctuation factors derived from mean monthly observations recorded by the tide gauge stations. This step enhances the dataset, allowing for a more continuous understanding of sea-level changes on a year-to-year basis.

To create localised sea-level forecasts, these monthly forecasts are linearly scaled using scaling factors derived from aligning the historical analyses from CMIP5 with the tide gauge observations.

These re-analyses combine weight factors detailed in table A.2 with the scaled model outputs, providing a sea-level re-analysis based on the 12 models across 11 locations scaled by the four tide gauge observations in the Gulf of Thailand.

4.4. Ground Deformation

The ground deformation analysis in this study focuses on projections for three key locations in Bangkok, as provided by Soonthornrangsan (2023). These locations are situ-

ated at longitudes 100.385°E, 100.532°E, and 100.600°E, and serve as the foundation for projecting ground deformations under a groundwater extraction rate of 500,000 m^3/day (Figure 4.2a). The projected ground deformations for these locations have been discussed in detail in Section 3.2.2 (Figure 3.9).

Interferometric Synthetic Aperture Radar (InSAR) measurements between October 2014 and March 2015 are used to establish ground deformation rates at the locations presented in Figure 4.2a. The deformation rates at multiple latitude points were recorded for each longitude, resulting in five land subsidence rates for 100.385°E, three for 100.532°E, and two for 100.596°E. This approach provided a detailed understanding of the deformation dynamics during this period.

I compared the observed deformation rates to those at locations LBKK026, LCSPK009, and LCSPK007 (numbered 1, 6, and 9 in Figure 4.2a). By analysing the Sentinel 1 satellite data over the 150-day period, the deformation rates were extrapolated to predict deformation for the year 2100 at the seven additional points. To cover a broader geographic area, the study area was divided into 44 rectangular polygons across the region (Figure 4.2b). This division allowed for a more detailed and accurate interpolation of subsidence rates. The polygons varied in size: those on the west side measured approximately 800 meters by 15.8 kilometres, central polygons were about 840 meters by 13.1 kilometres, and eastern polygons were roughly 830 meters by 6.5 kilometres.

The Sentinel 1 satellite data from October 2014 to March 2015 revealed higher subsidence rates in the western part of the study area compared to the central and eastern parts (Figure 4.3a).

Subsidence analysis for locations numbered as 1, 6, and 9 reveal similar trends over the 150-day period (Figure 4.3a). Significant differences are observed when the deformation is compared to the location south of points 1, 6 and 9. Location 1 recorded very low deformation during the 150-day observation period, in contrast to higher rates noted at the points along the same longitude. Consequently, interpolated forecasts predict very high rates of subsidence for areas south of location 1. Because the difference in subsidence rate is not that profound for locations 6-10, the subsidence forecast at these locations is much smaller than those south of location 1 (Figure 4.3b).

This approach provides a first and very basic framework for analysing and projecting ground deformation in Bangkok, considering both temporal and spatial variations in subsidence rates.

4.5. INTEGRATION OF LAND DEFORMATION DATA AND DEM ADAPTATION FOR SEA LEVEL RISE PROJECTIONS

Based on the land deformation approximations established for each polygon in the study area, the CoastalDEM v2.1 with elevation points from 2021 has been adapted to reflect the projected land subsidence. In this adaptation the projected land deformation values for each polygon have been deducted from the CoastalDEM v2.1. By deducting the estimated land deformation, the DEM will represent the anticipated topography of the area by the year 2100.

The adaptation of the DEM is necessary for roughly assessing which areas will could be subject to future flooding due to sea level rise. This adjusted DEM provides a more

(a) 10 locations where land deformation has been determined between October 2014 and March 2015.

(b) 44 polygons for which land deformation is projected in the year 2100.
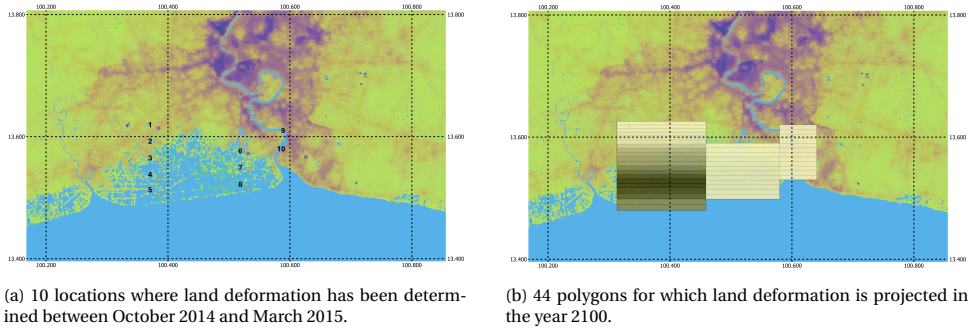
Figure 4.2: Population density coastal map of Bangkok and Samut Prakan

realistic foundation for subsequent flood risk analyses.

With the updated DEM, I performed a bathtub simulation to evaluate the impact of projected sea level rise on coastal areas. A bathtub simulation is a hydrodynamic modeling approach that identifies areas where the land elevation is below the projected sea level rise, indicating potential flooding zones. The sea level projections for 2100, determined earlier in this research, are overlaid on the new DEM to find these potential flooding zones.

The simulation reveals which coastal areas could be submerged or significantly affected by the projected sea level rise by 2100, taking into account the compounded effect of land subsidence.
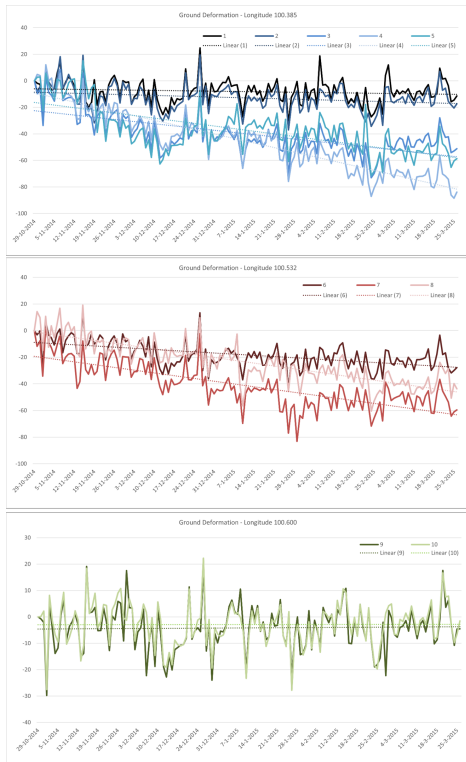
(a) Land deformation rate between 2014 and March 2015 for
the 10 selected locations from Sentinel 1 satellite.
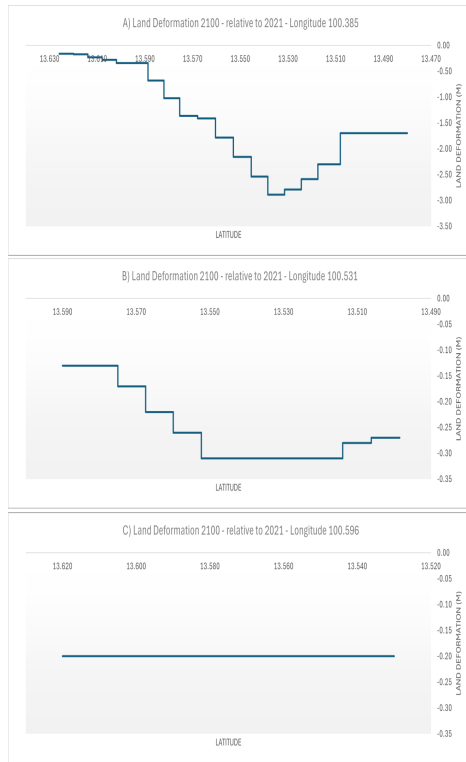
(b) Land deformation in meters in 2100 for the constructed
polygons relative to the year 2021.

5

INTEGRATION SEA-LEVEL RISE AND SUBSIDENCE

5.1. HISTORICAL GCM CORRECTION

The integration of monthly tide gauge data from four stations (Ko Sichang, Ko Lak, Ko Mattaphon, and Geting) was essential in refining sea level predictions. The normalised tide gauge data to the 2000 mean revealed consistent seasonal patterns, providing a foundation for bias correction. By aligning the historical GCM outputs with these observations in Section 4.1, the study ensured that projections accurately reflected local sea level changes influenced by both global climate trends and regional factors.

To correct the historical GCM outputs, in Section 4.1.2 multiple bias correction techniques were applied, namely linear scaling, variance scaling, and quantile mapping. With these methods I aimed to align the raw data with observed sea levels, enhancing the accuracy of the projections. The correction factors have been calculated by taking the average of the 12 models for each of the 11 locations in the Gulf. The correction factors used in the linear bias-correction are presented in Appendix B, in Figure B.2. Satellite altimetry data was then compared with the corrected models to validate the projections.

In Section 4.2 linear scaling emerged as the most reliable method among the three bias correction methods. It achieved an average R^2 value of 0.44, indicating that a substantial proportion of variance between observed and predicted values was captured. Additionally, the Mean Absolute Error (MAE) for this method averaged 67 mm, the lowest among the techniques tested, confirming linear scaling was most effective in minimising deviations from actual observed values. Based on the R^2 and the MAE, the linear scaling method can be appointed as the best method to provide accurate and reliable localised sea level predictions for the Gulf of Thailand (Figure 5.2a and 5.2b).

To demonstrate the trends across all models in the northern part of the GoT the MAE and the R^2 values have been determined (table 5.1). Models CCSM4 and GFDL-CM3 were selected for comparison. Model GFDL-CM3 was chosen for this comparison because the R^2 between the satellite altimetry and this adjusted model was the highest and
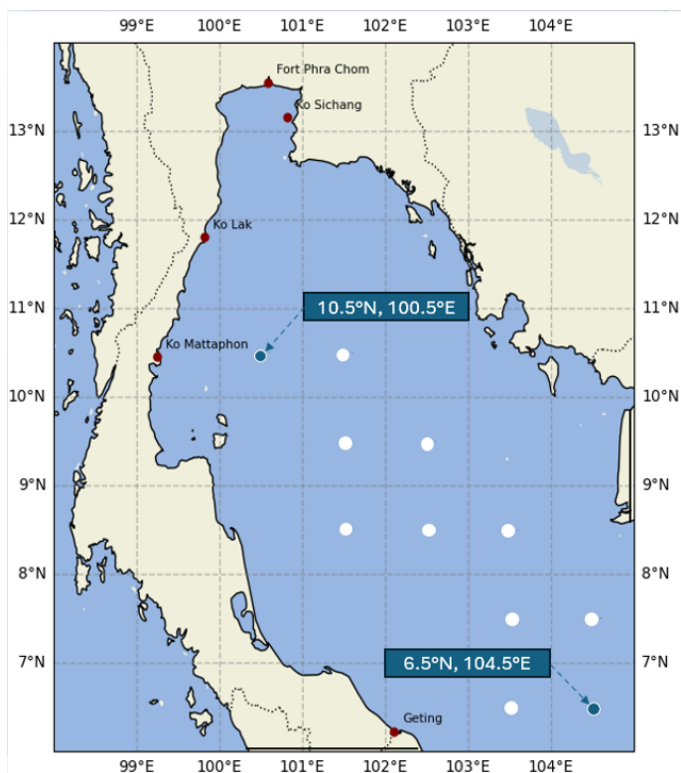
Figure 5.1: Representation of the GoT with the 11 locations at which sea level has been analysed. The locations (10.5°N, 100.5°E) and (6.5°N, 104.5°E) have been highlighted dark blue.

the MAE values the lowest among the 12 models. Model CCSM4 was chosen for comparison due to the lowest R^2 and the highest MAE in the northern part of the GoT.

The results indicate a better correlation between the corrected models and altimetry data as we move northward in the Gulf. For instance:

- **Model CCSM4:** At latitude 6.5°N, longitude 104.5°E (Figure 5.1), the correlation between the corrected model and the altimetry data is moderate, showing good alignment of seasonal and inter-annual variations but significant discrepancies in sea level amplitude Figure 5.3a). However, at latitude 10.5°N, longitude 100.5°E, the correlation improves, indicating higher accuracy in the northern regions (Figure 5.3b).

- **Model GFDL-CM3:** At latitude 6.5°N, longitude 104.5°E, similar to Model 2, the correlation is moderate but consistent patterns are observed (Figure 5.3c). At latitude 10.5°N, longitude 100.5°E, the correlation is strong, demonstrating better model performance in the north (Figure 5.3d).

These findings suggest that the bias correction methods applied are more effective in the northern parts of the Gulf. The integration of tide gauge data, historical GCM

Table 5.1: Mean Average Error and R^2 values at latitude 10.5°N and longitude 100.5°E for the Linear Scaling Method

Model ID	MAE	R^2	Model ID	MAE	R^2
1. CanESM2	66.82	0.67	7. IPSL-CM5A-LR	76.83	0.61
2. CCSM4	83.96	0.54	8. MIROC5	69.71	0.64
3. CNRM-CM5	54.85	0.78	9. MIROC-ESM	49.28	0.82
4. GFDL-CM3	49.45	0.83	10. MPI-ESM-LR	74.55	0.60
5. GISS-E2-R	61.41	0.73	11. MRI-CGCM3	47.10	0.83
6. HadGEM2-ES	58.23	0.74	12. NorESM1-M	58.59	0.76
Average	62.56	0.71			

outputs, and satellite altimetry has increased the reliability of sea level rise projections, providing a better understanding of future scenarios in the Gulf of Thailand.

(a) Coefficient of Determination (R^2)

(b) Mean Average Error (MAE)
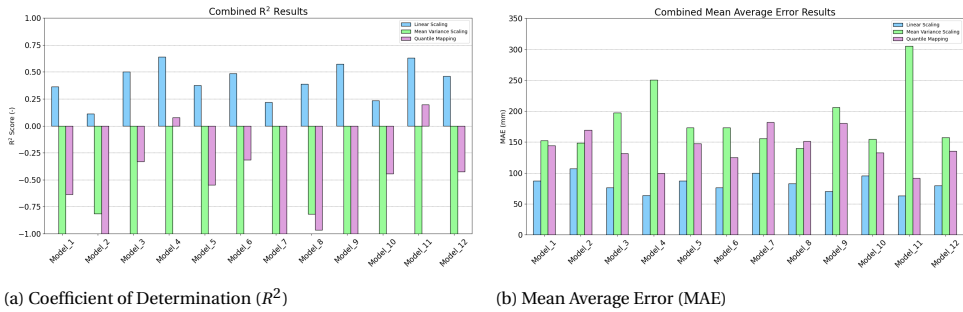
Figure 5.2: Statistical analysis between the extrapolated and scaled historical sea level predictions and the Copernicus satellite altimetry sea-level observations for each of the three correction methods.
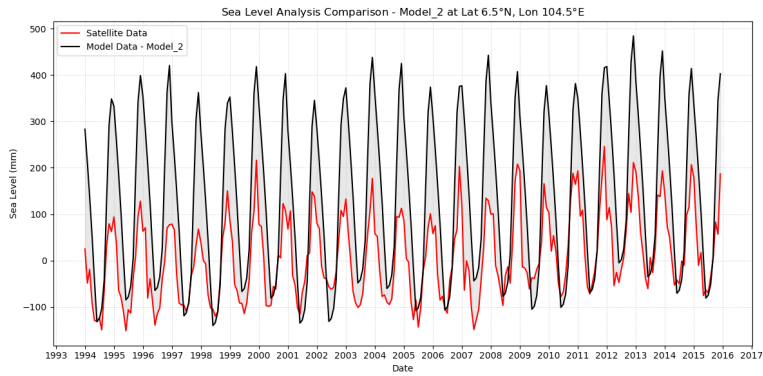
(a) CCSM4 - latitude 6.5°N, longitude 104.5°E
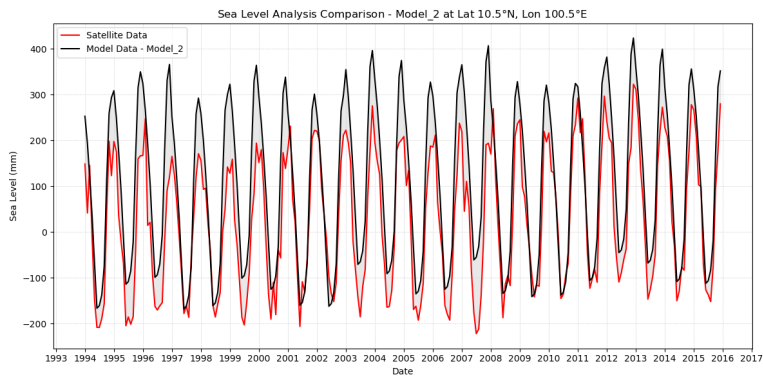
(b) CCSM4 - latitude 10.5°N, longitude 100.5°E
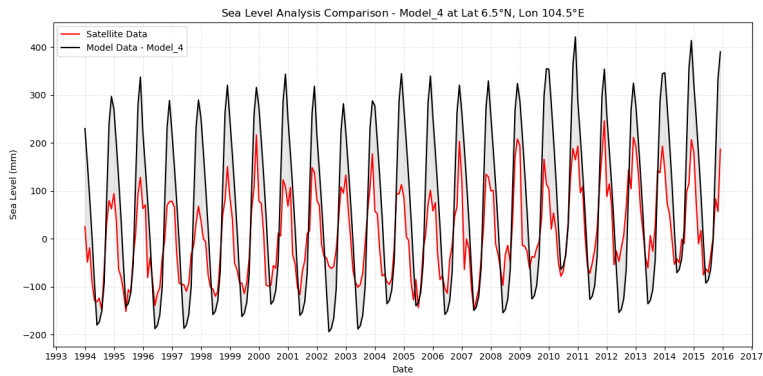
(c) GFDL-CM3 - latitude 6.5°N, longitude 104.5°E
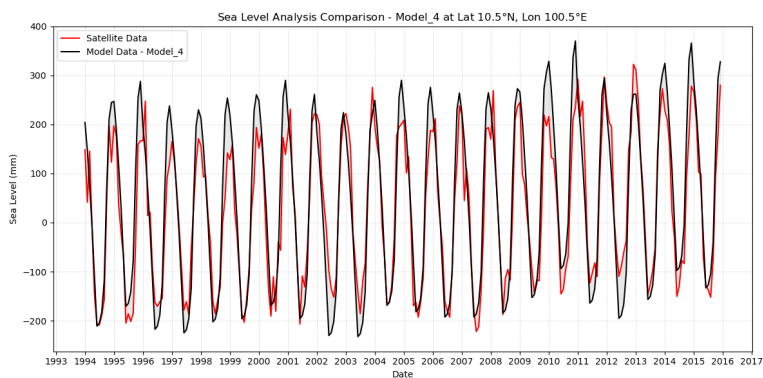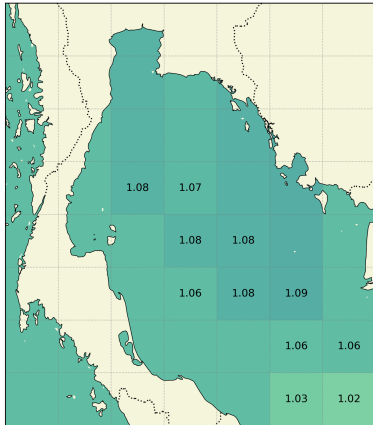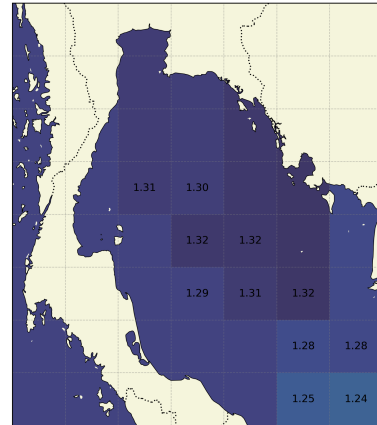
(a) Scenario SSP2-4.5   (b) Scenario SSP5-8.5

Figure 5.4: Projected sea level change in meters for December 2100 under both scenarios, relative to the average sea level between 1995 and 2014.

5.2. FUTURE SEA LEVEL PROJECTIONS

To provide a spatial understanding of the adjusted IPCC forecasts, future sea level forecasts for December 2100 were visualised on a grid-map of the Gulf of Thailand. These projections, scaled using linear scaling, were developed for scenarios SSP4.5 and SSP8.5.

Under the SSP4.5 scenario, a moderate increase in sea levels is projected, with values ranging from 1.02 to 1.09 meters across various locations in the Gulf (Figure 5.4a). In contrast, the SSP8.5 scenario predicts a more pronounced rise, with projections ranging from 1.24 to 1.31 meters (Figure 5.4b). Notably, the most significant increases are observed in the northern parts of the Gulf, particularly at coordinates 10.5°N, 100.5°E. This spatial variability highlights areas that may be more vulnerable to future sea level rise.

A time series analysis at location 10.5°N, 100.5°E reveals a gradual sea level rise between 2030 and 2100, based on 12 different CMIP5 models (Figures 5.5a and 5.5b). Under the SSP4.5 scenario, the projected median sea level rise is approximately 0.85 meters by 2100, with a 95% confidence level of 1.08 meters. The SSP8.5 scenario projects a median rise of about 1.1 meters, with a 95% confidence level of 1.31 meters by 2100 (Figures 5.5c and 5.5d).

These projections, adjusted to local tide gauge observations using the linear scaling method, reveal significant increases in sea level by 2100 for both emission scenarios. This analysis provides critical insights into anticipated changes in the Gulf of Thailand, supporting the development of targeted adaptation strategies for the region. The detailed spatial and temporal projections presented here underscore the importance of considering both regional variations and long-term trends in sea level rise when planning for future coastal management and climate adaptation measures in the Gulf of Thailand. The sea-level predictions in the northern part of the GoT are used for the coastal predictions hereafter.

5
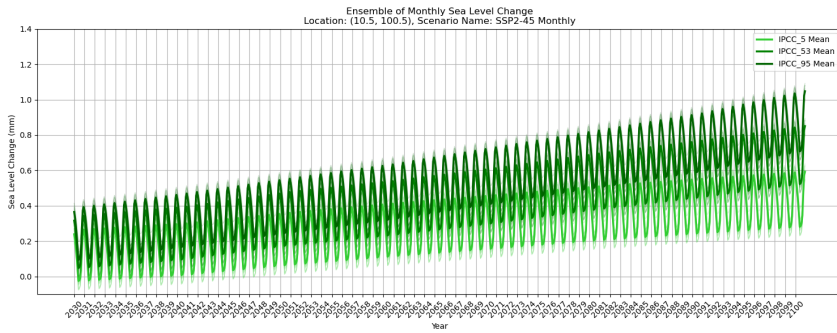
(a) Scenario SSP2-45 (2030 to 2100)
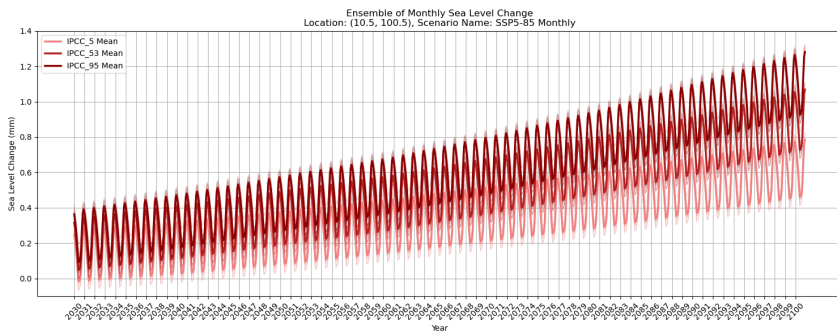
(b) Scenario SSP5-85 (2030 to 2100)
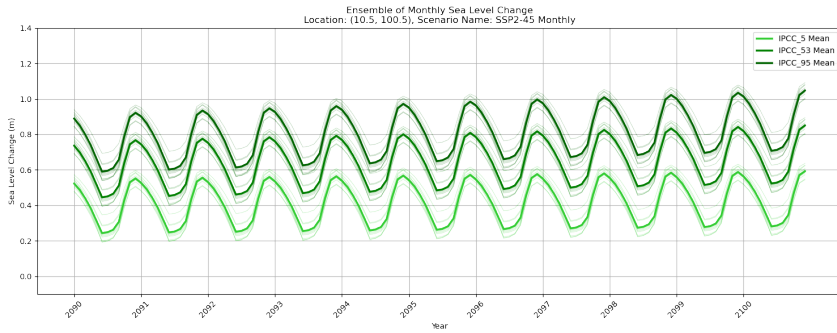
(c) Scenario SSP2-45 (2090 to 2100)
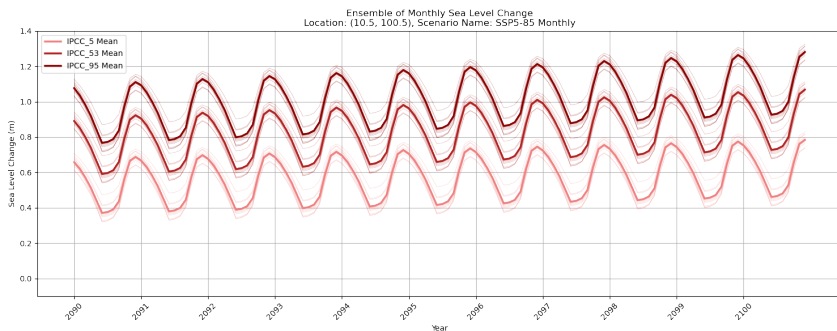
(d) Scenario SSP5-85 (2090 to 2100)

Figure 5.5: Monthly sea level projections at (10.5°N, 100.5°E) for IPCC AR6 scenarios, illustrating the variety in predictions based on different CMIP5 models and IPCC AR6 confidence intervals.

5.3. LAND DEFORMATION AND FLOODING

In this section, I have examined the interplay between land deformation and SLR, starting with an assessment of the impact of sea level rise alone, and then incorporating land deformation into the analysis. As a baseline for subsequent flooding simulations, Figure (5.6) represents the CoastalDEM in 2021 with the existing coastline.
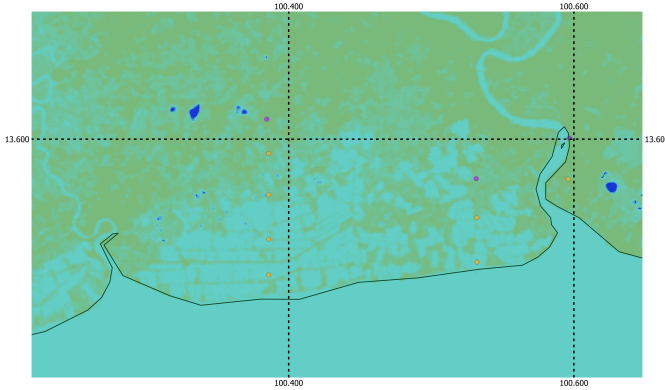
Figure 5.6: CoastalDEM v2.1 representing the initial coastal situation in 2021 upon which the flooding scenarios have been simulated.

5.3.1. SIMULATION RESULTS WITHOUT LAND SUBSIDENCE

The flooding scenarios were first run without accounting for land subsidence to isolate the impact of SLR. Three sea level scenarios were considered, consistent with the median projections of SSP4.5 (SLR of 0.85m) and SSP8.5 (SLR of 1.1m) and the 95% confidence projection of scenario SSP8.5 (SLR of of 1.31m):

Moderate Sea Level Rise (0.85 meters):   This scenario aligns with the median projection under the SSP4.5 scenario and simulated potential flooding impacts in the absence of land subsidence. The potential flooding area covers a substantial part of the current coastline of Samut Prakan. The simulation shows potential flooding primarily in low-lying areas which are mainly used for agriculture and fishing farms (Figure 5.7a). The area estimated to be flooded still contains clear elevated strokes of land.

Higher Sea Level Rise (1.1 meters):   Corresponding to the median projection under the SSP8.5, the results indicate a slightly greater risk of flooding, with slightly more areas at risk than in the previous scenario (Figure 5.7b). However, the area estimated to be flooded is very similar.

Upper Limit Sea Level Rise (1.31 meters):   This scenario, representing the 95% confidence interval under the SSP8.5, tests the upper limits of flooding risk without considering land deformation effects. It demonstrates potential flooding in low-lying regions and the strokes of elevated land in between the low-lying areas can be seen to be flooded more substantially (Figure 5.7c).

These initial simulations serve as a control group, helping to understand the additional impact of land subsidence when both factors are combined.

(a) Sea level rise of 0.85 meter

(b) Sea level rise of 1.10 meter

(c) Sea level rise of 1.30 meter
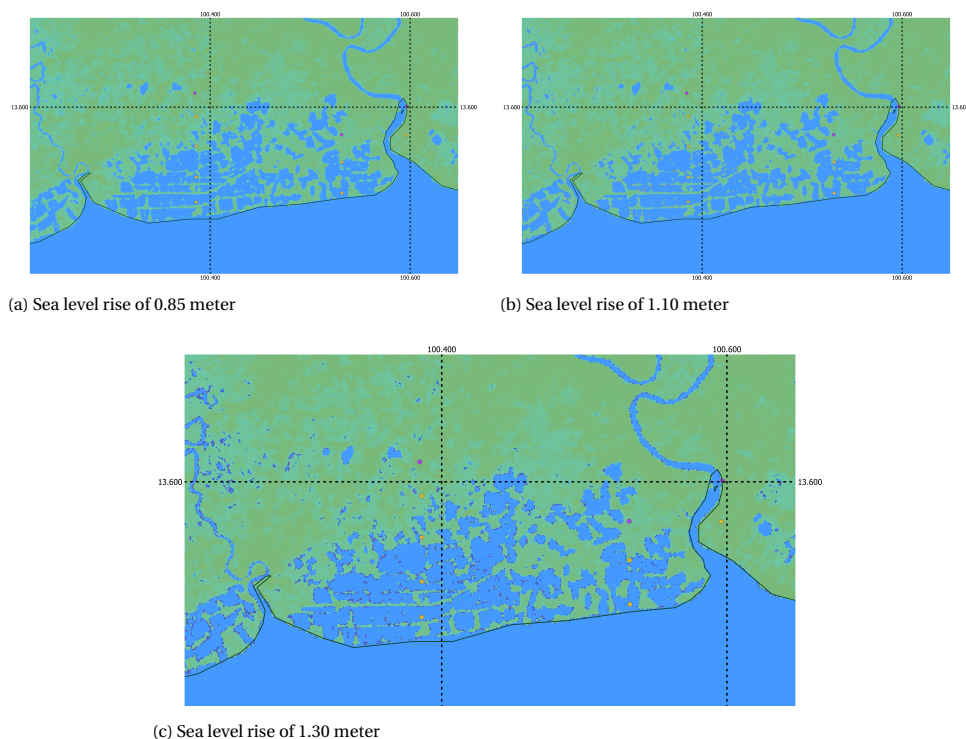
Figure 5.7: Projected coastline and flooded areas in Samut Prakan for the year 2100, based on the adjusted SLR scenario from the IPCC without land subsidence.

5.3.2. SIMULATION RESULTS WITH LAND SUBSIDENCE

Following the initial simulations, the CoastalDEM was adapted to account for previously estimated land deformation. This adjusted DEM serves as the foundation for a more complete flooding simulation, which overlays sea level rise scenarios upon the adapted DEM to identify potential flooding zones when both sea level rise and land subsidence are considered.

Moderate Sea Level Rise (0.85 meters):   With land subsidence taken into account, the areas at risk of flooding increase significantly, predominantly affecting the same low-
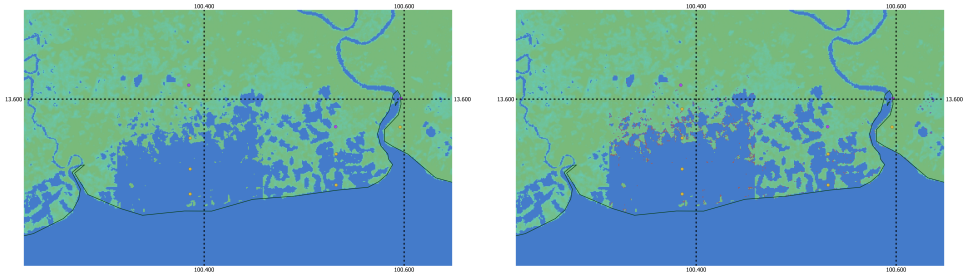
(a) Sea level rise of 0.85 meter with the estimated land deformation

(b) Sea level rise of 1.10 meter with the estimated land deformation
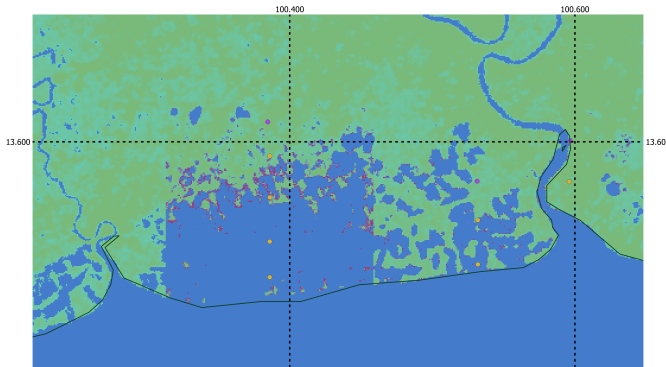
(c) Sea level rise of 1.31 meter with the estimated land deformation

Figure 5.8: Projected coastline and flooded areas in Samut Prakan for the year 2100, based on the adjusted SLR scenarios from the IPCC with estimated land subsidence.

lying agricultural regions (Figure 5.8a), however the elevated strokes of land in between the areas can clearly be seen to be at risk of flooding. The coastline has progressed land inwards substantially and the entire west side of the province is at risk of flooding.

Higher Sea Level Rise (1.1 meters): Under this scenario, the flooding area expands slightly more to the north than in the simulation of 0.85m with land subsidence incorporated (Figure 5.8b). This could mean that the more densely populated regions on the north side of the low-lying agricultural and fishing areas are under risk of flooding.

Upper Limit Sea Level Rise (1.31 meters): For this scenario, corresponding to the 95% confidence interval of SSP8.5, the results are similar to those of the 1.1-meter rise. Again, the potential flooding area extends land inwards and more populated areas could be under risk of flooding (Figure 5.8c).

6

DISCUSSION

In this study, I have examined the impacts of sea-level rise (SLR) and land subsidence on the northern part of the Gulf of Thailand. By localising CMIP5 model outputs with observed tide gauge data future sea level forecasts have been adjusted. A coastal DEM has been adjusted for future land subsidence. By combining these adjusted SLR forecasts with the adjusted DEM, potential areas at risk of flooding could be identified. Future sea level projections indicate that under high emission scenarios (SSP 8.5), the Gulf of Thailand may experience a sea-level rise of up to 1.31 meters by 2100. The risk of flooding due to SLR is intensified by the effects of subsidence in regions such as Bangkok. These projections suggest a critical need for coastal management strategies to mitigate potential risks.

The findings align with previous research by Trisirisatayawong et al. (2011) and Phienwej et al. (2006), which highlighted the compounded effects of sea-level rise and land subsidence in the Gulf of Thailand. Building on the methodologies suggested by Palmer et al. (2020) and Jaroenongard (2021), I've shown that sea-level analysis from GCMs could be bias-corrected with sea-level measurement data from local tide gauge station. By applying the calculated correction factors to global SLR forecasts, local SLR forecasts could be found.

An unexpected finding in this study was the small difference between flooding scenarios under various sea-level rise projections. Despite significant projected sea-level rise, the difference in the extent of flooding between the lower and upper scenarios was less pronounced than anticipated. This suggests that other factors, such as local topography and land subsidence, may play a more substantial role in determining the extend of flooding.

EXTENSION OF TIDE GAUGE DATA

One of the limitations of this research is the exclusion of tide gauge data from Fort Phrachula Chomklao due to significant land subsidence at the measurement site and the exclusion of data from all possible available tide gauge stations in the GoT. The exclusion of the

data from Fort Phrachula Chomlao was necessary to avoid distortions in sea-level measurements, as subsidence can significantly affect the relative sea level observed. Integrating land subsidence data at the tide gauge station could potentially make the tide gauge data usable. Together with the inclusion of more tide gauge station data the overall accuracy of the research could be increased.

LOCALISATION OF GLOBAL CIRCULATION MODELS FOR THE GULF OF THAILAND

The observed differences in sea level fluctuations between the northern and southern parts of the Gulf of Thailand underscore the importance of localising global sea level rise predictions. While our study primarily relied on tide gauge observations to linearly scale GCM predictions, several regional factors could be incorporated to refine these models for the Gulf of Thailand:

Seasonal Monsoon Winds: Monsoon winds significantly impact sea levels in the Gulf of Thailand, with northeast winds in winter pushing water into the gulf and southwest winds in summer having the opposite effect. While GCMs do simulate large-scale monsoon wind patterns, their coarse resolution often limits accurate representation of local wind-driven sea level fluctuations. Moreover, the precise interplay between monsoon winds and water movement in the Gulf may not be fully captured by these models. To improve sea level fluctuations in this region, the parameterisation of wind-water interactions in the GCMs should be investigated further.

Bathymetry: The shallower northern part of the Gulf is more susceptible to wind-driven changes in sea level compared to the deeper southern part (Yanagi et al., 2001). Integrating detailed bathymetric data into GCMs could increase spatial resolution of sea level predictions. However, many global climate models often lack the resolution to incorporate detailed local bathymetry, especially in regions with complex coastal features. This limitation can affect the accuracy of regional sea level projections in areas with varying depths like the Gulf of Thailand (Cannaby et al., 2016; Holt et al., 2017).

River Discharge: Freshwater input from rivers, particularly in the northern Gulf, affects local sea levels seasonally. Including river discharge data in GCMs could improve predictions of intra-annual sea level variations. Studies have shown that river discharge significantly influences sea levels along coastal regions. For instance, Piecuch et al. (2018) demonstrated that discharge from rivers within the Chesapeake Bay is significantly correlated with sea levels at coastal regions. Similarly, Gong and Shen (2011) found that freshwater discharge from major rivers contributes substantially to sea level variations in estuarine systems. Integrating river discharge dynamics into GCMs could enhance the ability of the models to predict seasonal and intra-annual sea level fluctuations, particularly in areas with significant freshwater input like the Gulf of Thailand.

By integrating these regional factors into GCMs, we could potentially develop more accurate and localised sea level rise predictions for the Gulf of Thailand. This approach would move beyond simple linear scaling of global predictions based on tide gauge observations, offering a more nuanced understanding of future sea level changes in the region. Future research should focus on quantifying the relative importance of these factors and developing methodologies to incorporate them into existing GCMs.

REFINEMENT OF LAND SUBSIDENCE PROJECTIONS

In this study, I have incorporated land subsidence projections as rectangular land areas, leading to abrupt changes in the subsidence values across the study areas. While this method provides a basic understanding of spatial variability, it lacks the granularity needed for precise coastal management planning. Future research should focus on developing more granular land subsidence maps to reflect the continuous nature of subsidence processes more accurately.

To achieve this, an increased density of GPS monitoring stations is essential for providing precise measurements of vertical land motion. Additionally, improved access to In-SAR data would increase the spatial resolution of subsidence measurements. This would allow for continuous monitoring across larger areas. Periodic levelling campaigns using surveying equipment would complement the GPS stations and InSAR data methods by providing data that has been verified by ground measurements to validate satellite measurements. By integrating these different data sources and establishing a long-term monitoring program, future research could produce more accurate land subsidence maps.

FUTURE RESEARCH DIRECTIONS

Future research could analyse the socio-economic impact of SLR and land subsidence in the area between Bangkok and the coast. Saltwater intrusion into low-lying grassland could be analysed, together with the effect of rising sea levels for the shallow water fishing farms. A population density examination of the area that is estimated to be flooded by 2100, could provide more clear image of the amount of people at risk. Assessing the socio-economic impacts of SLR and land subsidence will provide a more comprehensive understanding of the challenges and inform more effective adaptation strategies.

By addressing these research needs, we can improve the predictive capabilities of SLR models and develop more effective strategies to protect coastal regions from the impacts of climate change. This study lays the foundation for future research efforts aimed at enhancing the resilience of the Gulf of Thailand to rising sea levels and land subsidence.

6

7

CONCLUSION

In this chapter the main findings of this study have been brought together and the research question and sub-questions posed in the introduction have been addressed directly. The aim is to provide a clear understanding of how relative sea-level rise, combined with local land subsidence, will impact the coastline in Samut Prakan.

HOW WILL RELATIVE SEA-LEVEL RISE, CONSIDERING BOTH UNCERTAINTIES IN CLIMATE CHANGE AND LOCAL LAND SUBSIDENCE, AFFECT THE COASTLINE IN THE PROVINCE OF SAMUT PRAKAN?

The study has demonstrated that relative sea-level rise in the Gulf of Thailand is significantly influenced by both global climate change and local land subsidence. The combined effect of these factors results in higher sea levels and increased coastal flooding risk, particularly in low-lying areas. The integration of bias-corrected CMIP5 model outputs with observed tide gauge data has provided a robust framework for projecting future sea levels. These projections indicate that, under high emission scenarios (SSP 8.5), the Gulf of Thailand could experience a sea-level rise of up to 1.3 meters by 2100, exacerbating the impact of subsidence in regions like Bangkok.

SUB-QUESTION 1: WHAT ARE THE HISTORICAL RATES OF RELATIVE SEA-LEVEL RISE OBSERVED IN THE GULF OF THAILAND?

Historical data from tide gauges indicate that the Gulf of Thailand has experienced a relative sea-level rise at an average rate of approximately 1.7 mm/year over the past century. This rate has increased in recent decades, reaching about 3.3 mm/year since 1993. The historical analysis highlighted seasonal variations influenced by monsoon winds, with higher sea levels during the northeast monsoon and lower levels during the southwest monsoon. These findings underscore the need to account for both long-term trends and seasonal fluctuations in sea-level projections.

SUB-QUESTION 2: HOW CAN CMIP5 HISTORIC MODEL OUTPUTS BE COMBINED WITH OB-
SERVED TIDE GAUGE DATA TO ADJUST FOR LOCAL CIRCUMSTANCES?

The combination of CMIP5 model outputs with observed tide gauge data was achieved through bias correction methods, namely Linear Scaling, Variance Scaling, and Quantile Mapping. These methods adjusted the model outputs to better reflect local conditions, correcting for systemic biases and ensuring the predictions align with observed sea levels. The Linear Scaling method proved most effective, providing the highest correlation with observed data and the lowest mean absolute error. This approach allowed for accurate local projections that consider both global climate model predictions and local observational data.

SUB-QUESTION 3: HOW DOES THE SEA-LEVEL RANGE OF THESE ADJUSTED OUTPUTS IN-
FORM US ABOUT THE EXPECTED LOCAL SEA-LEVEL CHANGES GIVEN THE SSP 4.5 AND SSP
8.5 SCENARIOS, AND HOW CAN THESE PROJECTIONS BE EXPRESSED IN TERMS OF CONFID-
ENCE INTERVALS?

The adjusted outputs revealed that under SSP4.5, the Gulf of Thailand could see a sea-level rise of approximately 1.1 meters by 2100 at the 95% confidence interval. Under the more extreme SSP8.5 scenario, sea levels could rise by up to 1.31 meters at the 95% confidence interval. These projections were also expressed in terms of confidence intervals 5% and 50% providing a range of potential outcomes and capturing the uncertainties inherent in climate modeling. Under SSP4.5, we could expect a sea-level rise of 0.6 meters and 0.85 meters for intervals 5% and 50%, respectively. Under SSP8.5, we could expect a sea-level rise of 0.85 meters and 1.1 meters for intervals 5% and 50%, respectively The use of ensemble modeling further refined these projections, illustrating the variability and consensus among the different climate models.

SUB-QUESTION 4: BASED ON THE ADJUSTED SEA-LEVEL RISE PROJECTIONS AND LAND
SUBSIDENCE SCENARIOS, WHAT COASTLINE SCENARIOS CAN BE EXPECTED FOR THE GULF
OF THAILAND AND WHAT WOULD BE THE PROBABILITY FOR THESE SCENARIOS?

The integration of sea-level rise projections with land subsidence scenarios indicated significant risks for coastal flooding in the northern part of the Gulf of Thailand. By 2100, extensive areas in southern Bangkok could be submerged, with land subsidence exacerbating the effects of rising sea levels. The areas at risk of flooding under the scenarios investigated in this research area predominantly low-lying, agricultural regions with a low population density. In this study a DEM is used to simulate future flood risks, identifying critical zones that require targeted adaptation strategies. The probability of these scenarios was assessed through a combination of model outputs and historical data, providing a estimated view of future coastal vulnerabilities.

In conclusion, this research has provided insights into the combined impacts of sea-level rise and land subsidence in the northern part of the Gulf of Thailand. The findings highlight the urgent need for adaptive coastal management strategies to mitigate the risks and enhance the resilience of vulnerable coastal communities.

A

HAVERSINE DISTANCE CALCULATIONS

Table A.1: Distance in km between climate model locations and tide gauge observation stations in the Gulf of Thailand calculated by the Haversine formula.

Climate Model locations		Tide Gauge stations			
Longitude	Latitude	Ko Sichang	Ko Lak	Ko Mattaphon	Geting
100.5	10.5	297 km	163 km	137 km	507 km
101.5	8.5	522 km	411 km	328 km	262 km
101.5	9.5	413 km	315 km	268 km	370 km
101.5	10.5	304 km	234 km	246 km	480 km
102.5	8.5	549 km	470 km	417 km	257 km
102.5	9.5	445 km	389 km	371 km	367 km
103.5	6.5	796 km	715 km	641 km	157 km
103.5	7.5	693 km	626 km	570 km	209 km
103.5	8.5	594 km	545 km	514 km	296 km
104.5	6.5	842 km	782 km	725 km	266 km
104.5	7.5	746 km	701 km	663 km	300 km

Table A.2: Weight factor used for the implementation of the correction factors between the climate model locations and tide gauge observation stations in the Gulf of Thailand calculated by equation (4.6)

Climate Model locations		Tide Gauge stations			
Longitude	Latitude	Ko Sichang	Ko Lak	Ko Mattaphon	Geting
100.5	10.5	0.107	0.355	0.502	0.037
101.5	8.5	0.109	0.177	0.277	0.436
101.5	9.5	0.158	0.271	0.374	0.196
101.5	10.5	0.217	0.366	0.330	0.087
102.5	8.5	0.115	0.157	0.200	0.528
102.5	9.5	0.191	0.251	0.275	0.282
103.5	6.5	0.034	0.042	0.052	0.872
103.5	7.5	0.068	0.084	0.101	0.748
103.5	8.5	0.132	0.157	0.177	0.533
104.5	6.5	0.074	0.086	0.100	0.740
104.5	7.5	0.104	0.118	0.132	0.646

B

HISTORICAL SEA LEVEL ANALYSIS
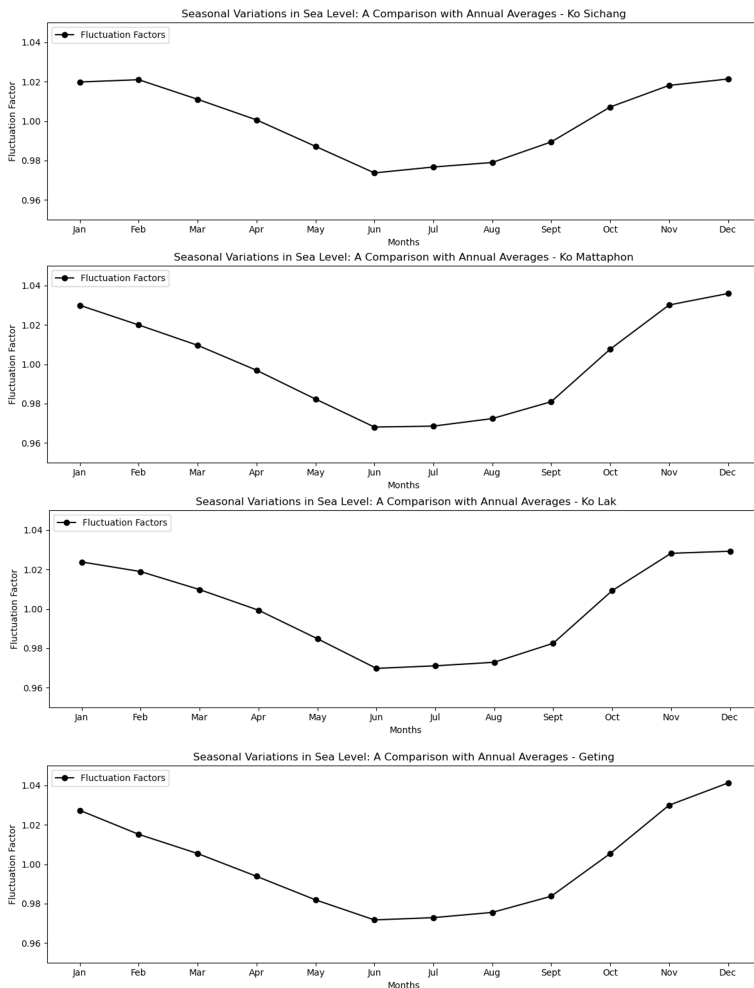
Figure B.1: Fluctuation Factors calculated from the tide gauge measurements to extrapolate the yearly SLR predictions from the IPCC and CMIP5 to monthly data analysis.

B

Longitude	101.5	100.5	102.5	101.5	103.5	102.5	101.5	104.5	103.5	104.5	103.5
Latitude	10.5	10.5	9.5	9.5	8.5	8.5	8.5	7.5	7.5	6.5	6.5
January	188	192	196	194	207	207	204	213	217	217	222
February	161	159	163	161	167	166	163	170	169	170	170
March	117	114	119	117	123	122	119	126	125	127	125
April	65	61	68	65	72	70	66	75	73	75	72
May	2	-4	7	3	13	11	6	18	17	19	16
June	-62	-70	-52	-58	-41	-43	-51	-34	-34	-31	-33
July	-55	-65	-46	-53	-35	-38	-46	-28	-28	-25	-27
August	-43	-52	-34	-40	-23	-25	-33	-16	-16	-13	-15
September	-1	-10	7	1	16	14	7	22	22	25	23
October	109	107	113	110	119	118	114	123	123	124	124
November	195	199	203	201	216	215	212	222	227	226	233
December	213	218	228	225	250	250	244	260	269	268	280

Figure B.2: The correction factors in mm calculated during the linear bias-correction of the CMIP5 sea level models by the tide gauge observations. This table contains the average values from all of the 12 CMIP5 models. These factors have been used for the adjustment of the IPCC AR6 sea level forecasts.
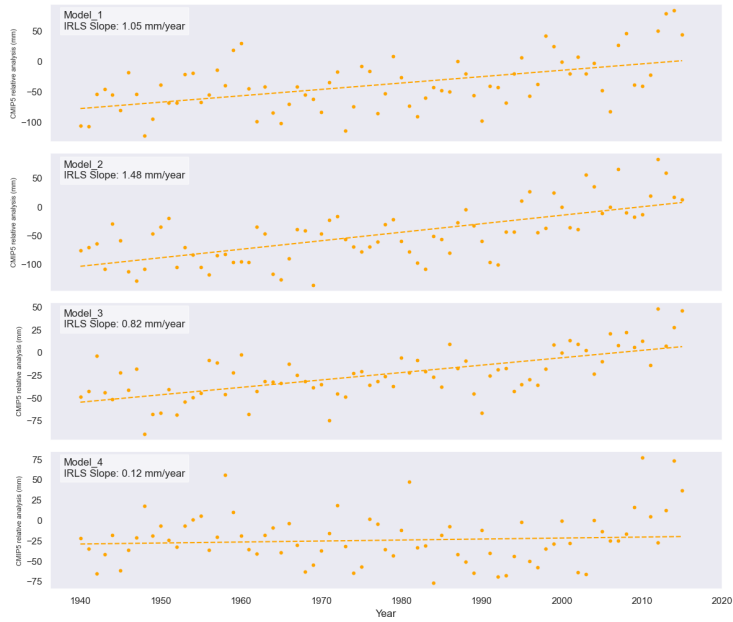
Figure B.3: CMIP5 historical sea level simulations at coordinates (10.5°N, 100.5°E). These sea level outputs have been extrapolated and bias-corrected with the local tide gauge measurements
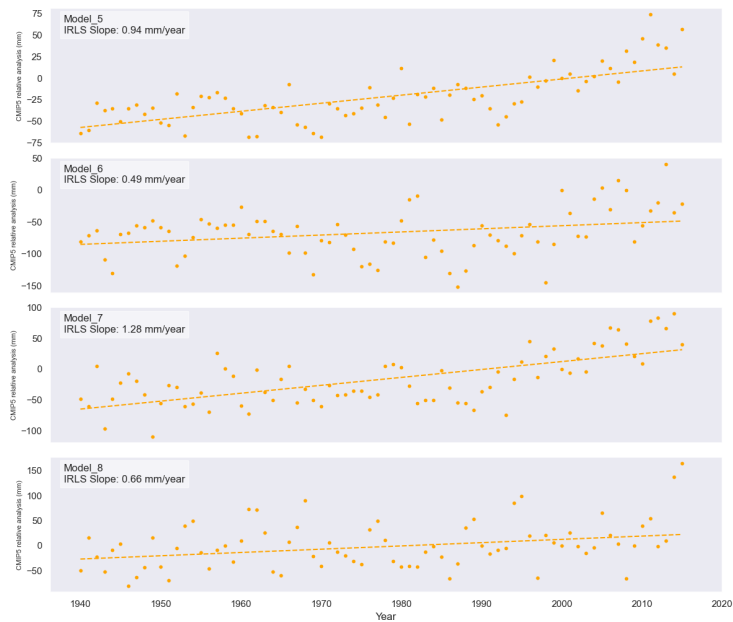
Figure B.4: CMIP5 historical sea level simulations at coordinates (10.5°N, 100.5°E). These sea level outputs have been extrapolated and bias-corrected with the local tide gauge measurements
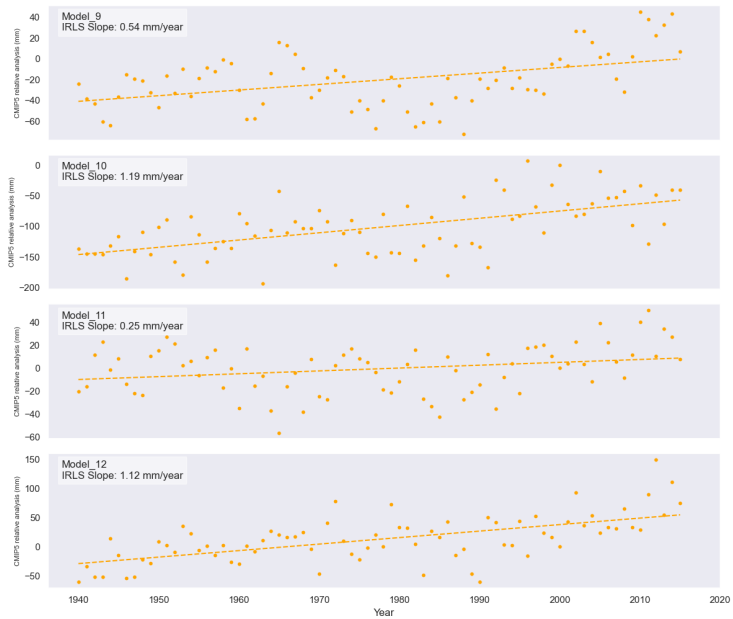
Figure B.5: CMIP5 historical sea level simulations at coordinates (10.5°N, 100.5°E). These sea level outputs have been extrapolated and bias-corrected with the local tide gauge measurements

Arora, V. K., Scinocca, J. F., Boer, G. J., Christian, J. R., Denman, K. L., Flato, G. M., Kharin, V. V., Lee, W. G., & Merryfield, W. J. (2011). Carbon emission limits required to satisfy future representative concentration pathways of greenhouse gases. *Geophysical Research Letters*, *38*(5). https://doi.org/10.1029/2010GL046270

Cannaby, H., Palmer, M. D., Howard, T., Bricheno, L., Calvert, D., Krijnen, J., Wood, R., Tinker, J., Bunney, C., Harle, J., Saulter, A., O'Neill, C., Bellingham, C., & Lowe, J. (2016). Projected sea level rise and changes in extreme storm surge and wave events during the 21st century in the region of Singapore. *Ocean Science*, *12*(3), 613–632. https://doi.org/10.5194/os-12-613-2016

Cannon, A. J., Sobie, S. R., & Murdock, T. Q. (2015). Bias Correction of GCM Precipitation by Quantile Mapping: How Well Do Methods Preserve Changes in Quantiles and Extremes? *Journal of Climate*, *28*(17), 6938–6959. https://doi.org/10.1175/JCLI-D-14-00754.1

Church, J. A., & White, N. J. (2011). Sea-Level Rise from the Late 19th to the Early 21st Century. *Surveys in Geophysics*, *32*(4-5), 585–602. https://doi.org/10.1007/s10712-011-9119-1

Collins, W. J., Bellouin, N., Doutriaux-Boucher, M., Gedney, N., Halloran, P., Hinton, T., Hughes, J., Jones, C. D., Joshi, M., Liddicoat, S., Martin, G., O'Connor, F., Rae, J., Senior, C., Sitch, S., Totterdell, I., Wiltshire, A., & Woodward, S. (2011). Development and evaluation of an Earth-System model - HadGEM2. *Geoscientific Model Development*, *4*(4), 1051–1075. https://doi.org/10.5194/gmd-4-1051-2011

Copernicus Climate Change Service, C. D. S. (2018). Sea level gridded data from satellite observations for the global ocean from 1993 to present. https://doi.org/10.24381/cds.4c328c78

Dean, R. G., & Houston, J. R. (2013). Recent sea level trends and accelerations: Comparison of tide gauge and satellite results. *Coastal Engineering*, *75*, 4–9. https://doi.org/10.1016/j.coastaleng.2013.01.001

Delworth, T. L., Broccoli, A. J., Rosati, A., Stouffer, R. J., Balaji, V., Beesley, J. A., Cooke, W. F., Dixon, K. W., Dunne, J., Dunne, K. A., Durachta, J. W., Findell, K. L., Ginoux, P., Gnanadesikan, A., Gordon, C. T., Griffies, S. M., Gudgel, R., Harrison, M. J., Held, I. M., . . . Zhang, R. (2006). *GFDL's CM2 Global Coupled Climate Models. Part I: Formulation and Simulation Characteristics* (tech. rep.). http://nomads.gfdl.noaa.gov/

Dufresne, J. L., Foujols, M. A., Denvil, S., Caubel, A., Marti, O., Aumont, O., Balkanski, Y., Bekki, S., Bellenger, H., Benshila, R., Bony, S., Bopp, L., Braconnot, P., Brockmann, P., Cadule, P., Cheruy, F., Codron, F., Cozic, A., Cugnet, D., . . . Vuichard, N. (2013). Climate change projections using the IPSL-CM5 Earth System Model: From CMIP3 to CMIP5. *Climate Dynamics*, *40*(9-10), 2123–2165. https://doi.org/10.1007/s00382-012-1636-1

Fox-Kemper, B., Hewitt, H. T., & Xiao, C. (2023). Ocean, Cryosphere and Sea Level Change. In *Climate change 2021 – the physical science basis* (pp. 1211–1362). Cambridge University Press. https://doi.org/10.1017/9781009157896.011

Gent, P. R., Danabasoglu, G., Donner, L. J., Holland, M. M., Hunke, E. C., Jayne, S. R., Lawrence, D. M., Neale, R. B., Rasch, P. J., Vertenstein, M., Worley, P. H., Yang, Z. L., & Zhang, M. (2011). The community climate system model version 4. *Journal of Climate, 24*(19), 4973–4991. https://doi.org/10.1175/2011JCLI4083.1

Gong, W., & Shen, J. (2011). The response of salt intrusion to changes in river discharge and tidal mixing during the dry season in the Modaomen Estuary, China. *Continental Shelf Research, 31*(7-8), 769–788. https://doi.org/10.1016/j.csr.2011.01.011

Holgate, S. J., Matthews, A., Woodworth, P. L., Rickards, L. J., Tamisiea, M. E., Bradshaw, E., Foden, P. R., Gordon, K. M., Jevrejeva, S., & Pugh, J. (2013). New data systems and products at the permanent service for mean sea level. *Journal of Coastal Research, 29*(3), 493–504. https://doi.org/10.2112/JCOASTRES-D-12-00175.1

Holt, J., Hyder, P., Ashworth, M., Harle, J., Hewitt, H. T., Liu, H., New, A. L., Pickles, S., Porter, A., Popova, E., Allen, J. I., Siddorn, J., & Wood, R. (2017). Prospects for improving the representation of coastal and shelf seas in global ocean models. *Geoscientific Model Development, 10*(1), 499–523. https://doi.org/10.5194/gmd-10-499-2017

Intergovernmental Panel on Climate Change. (2023, June). Ocean, Cryosphere and Sea Level Change. In *Climate change 2021 – the physical science basis* (pp. 1211–1362). Cambridge University Press. https://doi.org/10.1017/9781009157896.011

Jaroenongard, C., Babel, M. S., Shrestha, S., Weesakul, S., Nitivattananon, V., & Khadka, D. (2021). Projecting relative sea level rise under climate change at the phrachula chomklao fort tide gauge in the upper gulf of Thailand. *Water (Switzerland), 13*(12). https://doi.org/10.3390/w13121702

Kulp, S., & Strauss, B. (2023). *CoastalDEM v2.1: A high-accuracy and -resolution global coastal elevation model trained on ICESat-2 lidar*. http://www.climatecentral.org/coastaldem-v2.1.

Lee, H., & Romero, J. (2023). *Climate Change 2023: Synthesis Report. Contribution of Working Groups I, II and III to the Sixth Assessment Report of the Intergovernmental Panel on Climate Change* (tech. rep.). https://www.researchgate.net/publication/370465535

Naeije, M. C., Simons, W. J., Pradit, S., Niemnil, S., Thongtham, N., Mustafar, M. A., & Noppradit, P. (2022). Monitoring Megathrust-Earthquake-Cycle-Induced Relative Sea-Level Changes near Phuket, South Thailand, Using (Space) Geodetic Techniques. *Remote Sensing, 14*(20). https://doi.org/10.3390/rs14205145

Nerem, R. S., Frederikse, T., & Hamlington, B. D. (2022). Extrapolating Empirical Models of Satellite-Observed Global Mean Sea Level to Estimate Future Sea Level Change. *Earth's Future, 10*(4). https://doi.org/10.1029/2021EF002290

O'Neill, B. C., Kriegler, E., Riahi, K., Ebi, K. L., Hallegatte, S., Carter, T. R., Mathur, R., & van Vuuren, D. P. (2014). A new scenario framework for climate change research:

The concept of shared socioeconomic pathways. *Climatic Change*, *122*(3), 387–400. https://doi.org/10.1007/s10584-013-0905-2

Palmer, M. D., Domingues, C. M., Slangen, A. B. A., & Boeira Dias, F. (2021). An ensemble approach to quantify global mean sea-level rise over the 20th century from tide gauge reconstructions. *Environmental Research Letters*, *16*(4), 044043. https://doi.org/10.1088/1748-9326/abdaec

Palmer, M. D., Gregory, J. M., Bagge, M., Calvert, D., Hagedoorn, J. M., Howard, T., Klemann, V., Lowe, J. A., Roberts, C. D., Slangen, A. B., & Spada, G. (2020). Exploring the Drivers of Global and Local Sea-Level Change Over the 21st Century and Beyond. *Earth's Future*, *8*(9). https://doi.org/10.1029/2019EF001413

Phien-wej, N., Giao, P., & Nutalaya, P. (2006). Land subsidence in Bangkok, Thailand. *Engineering Geology*, *82*(4), 187–201. https://doi.org/10.1016/j.enggeo.2005.10.004

Phien-wej, N., Giao, P. H., & Nutalaya, P. (2006). Land subsidence in Bangkok, Thailand. *Engineering Geology*, *82*(4), 187–201. https://doi.org/10.1016/j.enggeo.2005.10.004

Piecuch, C. G., Bittermann, K., Kemp, A. C., Ponte, R. M., Little, C. M., Engelhart, S. E., & Lentz, S. J. (2018). River-discharge effects on United States Atlantic and Gulf coast sea-level changes. *Proceedings of the National Academy of Sciences*, *115*(30), 7729–7734. https://doi.org/10.1073/pnas.1805428115

Saramul, S. (2017). Seasonal Monsoon Variations in Surface Currents in the Gulf of Thailand Revealed by High Frequency Radar. *Engineering Journal*, *21*(4), 25–37. https://doi.org/10.4186/ej.2017.21.4.25

Saramul, S., & Ezer, T. (2014). Spatial variations of sea level along the coast of Thailand: Impacts of extreme land subsidence, earthquakes and the seasonal monsoon. *Global and Planetary Change*, *122*, 70–81. https://doi.org/10.1016/j.gloplacha.2014.08.012

Schmidt, G. A., Ruedy, R., Hansen, J. E., Aleinov, I., Bell, N., Bauer, M., Bauer, S., Cairns, B., Canuto, V., Cheng, Y. E., Genio, A. D., Faluvegi, G., Friend, A. D., Hall, T. M., Hu, Y., Kelley, M., Kiang, N. Y., Koch, D., Lacis, A. A., . . . Yao, M.-S. (2006). *Present-Day Atmospheric Simulations Using GISS ModelE: Comparison to In Situ, Satellite, and Reanalysis Data* (tech. rep.). http://www.giss.nasa.gov.

Sinnott, R. W. (1984). Virtues of the Haversine. *Sky Telesc,* 68–159.

Slangen, A. B. A., Carson, M., Katsman, C. A., van de Wal, R. S. W., Köhl, A., Vermeersen, L. L. A., & Stammer, D. (2014). Projecting twenty-first century regional sea-level changes. *Climatic Change*, *124*(1-2), 317–332. https://doi.org/10.1007/s10584-014-1080-9

Soonthornrangsan, J. T., Bakker, M., & Vossepoel, F. C. (2023). *Linked data-driven, physics-based modeling of groundwater and subsidence with application to Bangkok, Thailand* (tech. rep.).

Stevens, B., Giorgetta, M., Esch, M., Mauritsen, T., Crueger, T., Rast, S., Salzmann, M., Schmidt, H., Bader, J., Block, K., Brokopf, R., Fast, I., Kinne, S., Kornblueh, L., Lohmann, U., Pincus, R., Reichler, T., & Roeckner, E. (2013). Atmospheric component of the MPI-M earth system model: ECHAM6. *Journal of Advances in Modeling Earth Systems*, *5*(2), 146–172. https://doi.org/10.1002/jame.20015

Tebakari, T. (2020). Use of high-resolution elevation data to assess the vulnerability of the Bangkok metropolitan area to sea level rise. *Hydrological Research Letters*, *14*(4), 136–142. https://doi.org/10.3178/hrl.14.136

Terry, J. P., Jankaew, K., & Dunne, K. (2015). Coastal vulnerability to typhoon inundation in the Bay of Bangkok, Thailand? Evidence from carbonate boulder deposits on Ko Larn island. *Estuarine, Coastal and Shelf Science*, *165*, 261–269. https://doi.org/10.1016/j.ecss.2015.05.028

Teutschbein, C., & Seibert, J. (2012). Bias correction of regional climate model simulations for hydrological climate-change impact studies: Review and evaluation of different methods. *Journal of Hydrology*, *456-457*, 12–29. https://doi.org/10.1016/j.jhydrol.2012.05.052

Tjiputra, J. F., Roelandt, C., Bentsen, M., Lawrence, D. M., Lorentzen, T., Schwinger, J., Seland & Heinze, C. (2013). Evaluation of the carbon cycle components in the Norwegian Earth System Model (NorESM). *Geoscientific Model Development*, *6*(2), 301–325. https://doi.org/10.5194/gmd-6-301-2013

Trisirisatayawong, I., Naeije, M., Simons, W., & Fenoglio-Marc, L. (2011). Sea level change in the Gulf of Thailand from GPS-corrected tide gauge data and multi-satellite altimetry. *Global and Planetary Change*, *76*(3-4), 137–151. https://doi.org/10.1016/j.gloplacha.2010.12.010

Voldoire, A., Sanchez-Gomez, E., Salas y Mélia, D., Decharme, B., Cassou, C., Sénési, S., Valcke, S., Beau, I., Alias, A., Chevallier, M., Déqué, M., Deshayes, J., Douville, H., Fernandez, E., Madec, G., Maisonnave, E., Moine, M. P., Planton, S., Saint-Martin, D., ... Chauvin, F. (2013). The CNRM-CM5.1 global climate model: Description and basic evaluation. *Climate Dynamics*, *40*(9-10), 2091–2121. https://doi.org/10.1007/s00382-011-1259-y

Wahl, T., Haigh, I. D., Woodworth, P. L., Albrecht, F., Dillingh, D., Jensen, J., Nicholls, R. J., Weisse, R., & Wöppelmann, G. (2013, September). Observed mean sea level changes around the North Sea coastline from 1800 to present. https://doi.org/10.1016/j.earscirev.2013.05.003

Watanabe, M., Chikira, M., Imada, Y., & Kimoto, M. (2011). Convective control of ENSO simulated in MIROC. *Journal of Climate*, *24*(2), 543–562. https://doi.org/10.1175/2010JCLI3878.1

Watanabe, M., Suzuki, T., O'Ishi, R., Komuro, Y., Watanabe, S., Emori, S., Takemura, T., Chikira, M., Ogura, T., Sekiguchi, M., Takata, K., Yamazaki, D., Yokohata, T., Nozawa, T., Hasumi, H., Tatebe, H., & Kimoto, M. (2010). Improved climate simulation by MIROC5: Mean states, variability, and climate sensitivity. *Journal of Climate*, *23*(23), 6312–6335. https://doi.org/10.1175/2010JCLI3679.1

Yanagi, T., Sachoemar, S. I., Takao, T., & Fujiwara, S. (2001). Seasonal Variation of Stratification in the Gulf of Thailand. *Journal of Oceanography*, *57*(4), 461–470. https://doi.org/10.1023/A:1021237721368

Yukimoto, S., Adachi, Y., Hosaka, M., Sakami, T., Yoshimura, H., Hirabara, M., Tanaka, T. Y., Shindo, E., Tsujino, H., Deushi, M., Mizuta, R., Yabu, S., Obata, A., Nakano, H., Koshiro, T., Ose, T., & Kitoh, A. (2012). A new global climate model of the Meteorological Research Institute: MRI-CGCM3: -Model description and basic

performance-. *Journal of the Meteorological Society of Japan, 90*(A), 23–64. https://doi.org/10.2151/jmsj.2012-A02